Accepted Manuscript

Subduction or sagduction? Ambiguity in constraining the origin of ultramafic–mafic bodies in the Archean crust of NW Scotland

Tim E. Johnson, Michael Brown, Kathryn M. Goodenough, Chris Clark, Peter D. Kinny, Richard W. White

Please cite this article as: T.E. Johnson, M. Brown, K.M. Goodenough, C. Clark, P.D. Kinny, R.W. White, Subduction or sagduction? Ambiguity in constraining the origin of ultramafic–mafic bodies in the Archean crust of NW Scotland, *Precambrian Research* (2016), doi: http://dx.doi.org/10.1016/j.precamres.2016.07.013

Subduction or sagduction? Ambiguity in constraining the origin of ultramafic–mafic bodies in the Archean crust of NW Scotland

Tim E. Johnson[a*], Michael Brown[b], Kathryn M. Goodenough[c], Chris Clark[a], Peter D. Kinny[a] & Richard W. White[d]

[a] *Department of Applied Geology, The Institute for Geoscience Research (TIGeR), Curtin University, GPO Box U1987, Perth WA 6845, Australia*

[b] *Laboratory for Crustal Petrology, Department of Geology, University of Maryland, College Park, MD 20742-4211, USA*

[c] *British Geological Survey, West Mains Road, Edinburgh EH9 3LA, UK*

[d] *Earth System Science Research Centre, Institute for Geosciences, University of Mainz, Becherweg 21, D–55099, Mainz, Germany*

Corresponding author at: Department of Applied Geology, Curtin University, GPO Box U1987, Perth WA 6845, Australia.

Tel.: +61 8 92667332; fax: +61 8 92663153

E-mail address: tjohnson@uni-mainz.de (Tim Johnson)

Running title: LEWISIAN ULTRAMAFIC–MAFIC BODIES

1 **ABSTRACT**

2 The Lewisian Complex of NW Scotland is a fragment of the North Atlantic Craton. It

3 comprises mostly Archean tonalite–trondhjemite–granodiorite (TTG) orthogneisses that were

4 variably metamorphosed and reworked in the late Neoarchean to Palaeoproterozoic. Within

5 the granulite facies central region of the mainland Lewisian Complex, discontinuous belts

6 composed of ultramafic–mafic rocks and structurally overlying garnet–biotite gneiss (brown

7 gneiss) are spatially associated with steeply-inclined amphibolite facies shear zones that have

8 been interpreted as terrane boundaries. Interpretation of the primary chemical composition of

9 these rocks is complicated by partial melting and melt loss during granulite facies

10 metamorphism, and contamination with melts derived from the adjacent migmatitic TTG host

11 rocks. Notwithstanding, the composition of the layered ultramafic–mafic rocks is suggestive

12 of a protolith formed by differentiation of tholeiitic magma, where the ultramafic portions of

13 these bodies represent the metamorphosed cumulates and the mafic portions the

14 metamorphosed fractionated liquids. Although the composition of the brown gneiss does not

15 clearly discriminate the protolith, it most likely represents a metamorphosed sedimentary or

16 volcano-sedimentary sequence. For Archean rocks, particularly those metamorphosed to

17 granulite facies, the geochemical characteristics typically used for discrimination of

18 paleotectonic environments are neither strictly appropriate nor clearly diagnostic. Many of

19 the rocks in the Lewisian Complex have 'arc-like' trace element signatures. These signatures

20 are interpreted to reflect derivation from hydrated enriched mantle and, in the case of the

21 TTG gneisses, partial melting of amphibolite source rocks containing garnet and a Ti-rich

22 phase, probably rutile. However, it is becoming increasingly recognized that in Archean

23 rocks such signatures may not be unique to a subduction environment but may relate to

24 processes such as delamination and dripping. Consequently, it is unclear whether the

25 Lewisian ultramafic–mafic rocks and brown gneisses represent products of plate margin or

26 intraplate magmatism. Although a subduction-related origin is possible, we propose that an

27 intraplate origin is equally plausible. If the second alternative is correct, the ultramafic–mafic

28 rocks and brown gneisses may represent the remnants of intracratonic greenstone belts that

29 sank into the deep crust due to their density contrast with the underlying partially molten low

30 viscosity TTG orthogneisses.

31

32

33 **1. Introduction**

34

35   Archean cratons are predominantly composed of lower-grade granite–greenstone belts

36 and higher-grade grey gneiss terrains that may represent the upper and lower levels of ancient

37 continental crust (Windley and Bridgewater, 1971). In an alternative view, the high-grade

38 gneiss complexes and granite–greenstone belts have been interpreted as the ancient analogues

39 of modern active continental margins and back-arcs, respectively (Windley and Smith, 1976).

40 These different interpretations persist to the present day and are reflected in the 'subduction

41 versus sagduction' controversy for the formation of particular fragments of Archean crust,

42 such as the Barberton granite–greenstone belt (e.g., Kisters et al., 2003, 2010; Van

43 Kranendonk et al., 2014; Brown, 2015; Cutts et al., 2015).

44   Greenstone belts are linear to irregular in shape and generally synformal in structure,

45 comprising volcano-sedimentary successions (De Wit and Ashwal, 1997) that are surrounded

46 by dome-like composite batholiths of gneiss and granite (McGregor, 1951; Anhaeusser,

47 1975, 2014). Although lithologically complex and diverse in detail, greenstone belts are

48 dominated by (metamorphosed) basalt with other volcanic rocks ranging in composition from

49 ultramafic (komatiite) to felsic (dacite–rhyolite) and various sedimentary rocks that generally

50 become more abundant at shallower levels (Condie, 1994; De Wit and Ashwal, 1997;

51 Eriksson et al., 1997; Sylvester et al., 1997; Anhaeusser, 2014). Layered ultramafic–mafic

52 bodies may occur near the base of greenstone belts (Anhaeusser, 1975, 2001, 2014), which

53 has led some to interpret greenstone belts as dismembered fragments of obducted Archean

54 oceanic crust (ophiolites) and hence as evidence of subduction (De Wit et al., 1987; Kusky,

55 1990; Furnes et al., 2009; Hickman, 2012).

56   Grey gneiss terrains are dominated by felsic orthogneisses metamorphosed at

57 amphibolite to granulite facies, of which most (~70–75 vol.%) are tonalitic, trondhjemitic or

58 granodioritic (TTG) in composition (Moyen, 2011; Moyen and Martin, 2012). Commonly,

59 grey gneiss terrains include highly deformed layered ultramafic–mafic bodies and

60 supracrustal belts dominated by metavolcanic rocks. This association of rock types has been

61 interpreted by some to result from the dismemberment of oceanic island arcs formed at

62 convergent plate margins (e.g. Polat et al., 2015).

63   Although the archetypical dome-and-basin structure of Archean upper crust has been

64 regarded to be the result of polyphase folding during subhorizontal shortening (i.e. accretion;

65 e.g. Myers & Watkins, 1985; Blewett et al., 2002), this structure is more commonly

66 interpreted to reflect sinking, or 'sagduction' (Goodwin and Smith, 1980), of the overlying

67 greenstones and diapiric rise of gneisses and granitic plutons (Anhaeusser, 1975, 2014; Brun,

68 1980; Brun et al., 1981; Ramsay, 1989; Bouhallier et al., 1995; Kisters & Anhaeusser, 1995;

69 Chardon et al., 1996, 1998; Collins et al., 1998; Bremond d'Ars et al., 1999; Marshak, 1999;

70 Wellman, 2000; Sandiford et al., 2004; Van Kranendonk et al., 2004, 2014; Parmenter et al.,

71 2006; Robin and Bailey 2009; Thebaud and Rey 2013; François et al., 2014; Gapais et al.,

72 2014; Brown, 2015; Sizova et al., 2015). In many cases, rocks within grey gneiss terrains

73 have undergone polyphase deformation coeval with high-grade metamorphism at

74 suprasolidus conditions (Horie et al., 2011; Johnson et al., 2012, 2013). As a result,

75 establishing the relationship between the different lithological components, the origin of their

76 protoliths and the tectonic style poses challenges. However, if the dome-and-basin structure

77 of low-grade (greenschist to amphibolite facies) granite–greenstone terrains does reflect

78 diapirism and sagduction, then the disrupted remnants of the sinking greenstone belts might

79 be expected to occur in high-grade (amphibolite to granulite facies) gneiss terrains that

80 represent deeper levels in the Archean crust.

81 The evidence for subduction in the early Earth is based to a large degree on the 'arc-

82 like' geochemical signature preserved by many Archean volcanic rocks. Such signatures

83 indicate the rocks were derived from fluid-fluxed melting of mantle enriched in large-ion

84 lithophile elements (LILE) but depleted in high field-strength elements (HFSE), which is

85 commonly interpreted to record dehydration and/or partial melting of the downgoing slab and

86 concomitant enrichment of the overlying mantle wedge during subduction (e.g. Tatsumi,

87 2005; Jenner et al., 2009). However, it is becoming increasingly recognised that 'arc-like'

88 signatures may be generated in other geodynamic scenarios (Pearce, 2008; van Hunen and

89 Moyen, 2012) in which hydrated and enriched supracrustal material (e.g. sediment) is

90 transferred to the upper mantle. Recent geodynamic models for the early Earth, when the

91 mantle was much hotter, suggest that such non-uniformitarian scenarios are plausible

92 alternatives to subduction (Johnson et al., 2014; Sizova et al., 2015).

93 We use field observations combined with bulk-rock major oxide and trace element

94 compositional data to examine the origin of ultramafic–mafic–supracrustal bodies from the

95 Lewisian Complex of NW Scotland. An origin by subduction–accretion ('horizontal

96 tectonics') or by partial convective overturn ('vertical tectonics') is permissible within the

97 limitations of the data and the context of our current understanding of Archean crustal

98 dynamics. In these circumstances, resolution of the origin of the rocks comprising Archean

99 high-grade gneiss terrains may only be possible using geodynamic modelling informed by the

100 available geological data.

101

102

103   **2. Geological setting**

104

105   The Lewisian Complex of NW Scotland is a classic Precambrian high-grade grey

106   gneiss terrain. The rocks are mostly orthogneisses with Mesoarchean to Neoarchean protolith

107   ages that record a protracted history of magmatism, deformation and metamorphism spanning

108   more than a billion years (Kinny et al., 2005; Wheeler et al., 2010; Goodenough et al., 2013;

109   Crowley et al., 2015; Macdonald et al., 2015; Mason et al., 2015). The complex is dominated

110   by TTG gneisses within which occur abundant bodies of metamorphosed ultramafic–mafic

111   rocks and, locally, mica- and garnet-rich gneisses (Peach et al., 1907). The ultramafic–mafic

112   bodies range in shape and size from layered units several hundred metres across and several

113   kilometres in length to smaller metre-scale sheets and pods a few centimetres in diameter

114   (e.g. Bowes et al., 1964; Davies 1974; Sills et al., 1982; Rollinson & Fowler, 1987; Johnson

115   et al., 2012).

116   On the mainland, the Lewisian Complex comprises a granulite facies central region

117   bounded by regions to the north and south that record mainly amphibolite facies conditions

118   (Peach et al., 1907; Sutton and Watson, 1951; Fig. 1). Traditionally, the central region has

119   been interpreted to represent the deeper levels of a once-contiguous crustal block (e.g.

120   Sheraton et al., 1973; Park and Tarney, 1987). However, more recently, based on

121   geochronological studies, it has been proposed that the Lewisian Complex represents several

122   discrete crustal blocks (terranes) bounded by major shear zones, although the number of

123   terranes, the position of the terrane boundaries and the timing of their assembly is debated

124   (Kinny and Friend, 1997; Park et al., 2001; Kinny et al., 2005; Park, 2005; Goodenough et

125   al., 2010, 2013). To avoid any genetic connotations, we hereafter refer to the different

126 mainland 'terranes', as documented in Kinny et al. (2005), as 'blocks', following the usage of

127 Crowley et al. (2015).

128 In this section we review information pertaining to rocks in the central region

129 (comprising the Gruinard block in the south and the Assynt block in the north; Love et al.,

130 2004; Fig. 1) and describe the relationship between the northern part of the central region

131 (Assynt block) and the northern region (Rhiconich block; Kinny et al., 2005) across the

132 Laxford Shear Zone (Goodenough et al., 2010, 2013), where abundant large ultramafic–mafic

133 bodies and associated supracrustal rocks have been mapped in detail (BGS map sheets NC14

134 and NC24; Davies, 1976; see Fig. 2). Temporal constraints are summarised in Fig. 3. These

135 provides a foundation for the following two sections in which we provide details of the field

136 relations and chemical compositions of the ultramafic–mafic bodies and supracrustal rocks

137 occurring within the central region.

138

139 *2.1. Central region—protoliths and granulite facies (Badcallian) metamorphism*

140

141 Away from shear zones, central region TTG gneisses are characterised by a shallow-

142 to moderate-dipping gneissosity and recumbent tight-to-isoclinal folds (Wheeler et al., 2010).

143 The TTG gneisses preserve anhydrous (two pyroxene) mineral assemblages related to the

144 granulite facies metamorphic event (Badcallian; Park, 1970), which are variably overprinted

145 by amphibolite facies assemblages in which clinopyroxene and orthopyroxene are replaced

146 by hornblende and biotite, respectively.

147 Metabasic rocks preserve a variety of granulite facies mineral assemblages, with

148 many containing, in addition to pyroxenes and plagioclase, brown (Ti-rich) hornblende

149 and/or abundant garnet as part of the peak metamorphic mineral assemblage. Ultramafic

150 rocks are characterised by peak assemblages containing olivine, orthopyroxene,

7

151   clinopyroxene, brown hornblende and spinel, whose relative proportions vary (Johnson and

152   White, 2011). The mineral assemblages in this range of rock types are consistent with peak

153   metamorphic conditions of P = 0.8–1.2 GPa at T of >900 °C (Barnicoat, 1983; Cartwright

154   and Barnicoat, 1987; Sills and Rollinson, 1987; Johnson and White, 2011; Zirkler et al.,

155   2012; Johnson et al., 2013). Plagioclase, orthopyroxene and magnetite coronae replacing

156   garnet in metabasic rocks are interpreted to record limited near-isothermal retrograde

157   decompression to 0.7–0.9 GPa (Johnson & White, 2011). The absence of garnet in

158   metamorphosed ultramafic rocks, and the lack of evidence for its presence during prograde

159   metamorphism, suggests the rocks did not reach pressures higher than those recorded at the

160   metamorphic peak. Combined, these data are consistent with P–T paths that are tight

161   clockwise loops in which peak T coincided with peak P (Johnson and White, 2011, fig. 5b).

162   With the exception of ultramafic and rare calc-silicate rocks, granulite facies

163   metamorphism resulted in extensive partial melting and loss of melt (Johnson et al., 2012,

164   2013). Central region TTG gneisses show a distinctive depletion of large ion lithophile and

165   other mobile elements relative to rocks from the northern and southern regions (e.g. Sheraton

166   et al., 1973; Johnson et al., 2013, fig. 2). This depletion was related to the high-grade

167   metamorphism (Moorbath et al., 1969), with removal of mobile elements via the loss of

168   partial melt (O'Hara and Yarwood, 1978; Pride and Muecke, 1980, 1982; Cohen et al., 1991;

169   Johnson et al., 2012, 2013), although some of the differences reflect heterogeneities in the

170   original source composition (Rollinson and Tarney, 2005; Rollinson, 2012; Hughes et al.,

171   2014).

172   Around Scourie, Badcall and Kylestrome (Assynt block; Fig. 1), based on SHRIMP

173   U–Pb dating of zircon, the TTG gneisses have protolith (crystallisation) ages as old as c.

174   3.03–2.96 Ga (Friend and Kinny, 1995; Kinny and Friend, 1997), consistent with Sm–Nd

175   systematics (Hamilton et al., 1979). However, based on SIMS, SHRIMP and TIMS U–Pb

176   dating on zircon, younger protolith ages of *c.* 2.86-2.85 Ga have been suggested for some

177   gneisses within the Assynt block (Whitehouse and Kemp, 2010; Goodenough et al., 2013;

178   Crowley et al., 2015; Figs 2,3), which are similar to ages of *c.* 2.86–2.79 Ga inferred for

179   gneisses further south within the Gruinard block (Whitehouse et al., 1997; Corfu et al., 1998;

180   Love et al., 2004; Fig. 1).

181   The peak of Badcallian metamorphism in the Assynt block is inferred by some to

182   have occurred at *c.* 2.8–2.7 Ga (Fig. 3), based on TIMS U–Pb data from zircon (Corfu et al.,

183   1994) and *in situ* SIMS Pb–Pb data from a monazite inclusion in garnet (Zhu et al., 1997).

184   Others place the peak of high-grade metamorphism in the Assynt block at *c.* 2.49–2.48 Ga,

185   based on SHRIMP U–Pb data from zircon in the area north of Lochinver (Friend and Kinny,

186   1995; Kinny and Friend, 1997; Figs 1, 3). Corfu (2007) interprets these two groups of ages as

187   recording separate metamorphic events, which he correlated with the Badcallian and Inverian

188   (see below), respectively. Notwithstanding these interpretations, several studies have

189   indicated that samples of TTG gneiss from the Assynt block show a smear of zircon ages

190   along concordia between *c.* 3.0 and 2.5 Ga, in which individual metamorphic events are

191   difficult to identify (e.g. Whitehouse and Kemp, 2010), possibly reflecting variable Pb loss

192   from zircon during deformation and/or protracted cooling (e.g. Ashwal et al., 1999;

193   MacDonald et al., 2013). In a recent study using a technique involving partial dissolution of

194   thermally annealed morphologically complex zircon grains analysed by ID–TIMS, Crowley

195   et al. (2015) provide evidence in support of two high-grade metamorphic events in the Assynt

196   block, at *c.* 2.7 Ga and *c.* 2.5 Ga.

197   The peak of granulite facies metamorphism in the strongly retrogressed gneisses

198   further south in the central region, within the Gruinard block, is considered to have occurred

199   at c. 2.73 Ga (TIMS and SHRIMP U-Pb on zircon; Corfu et al., 1998; Love et al., 2004), with

200   no evidence for any later (c. 2.5 Ga) high-grade event. This led Corfu et al. (1998) to argue

9

201   that the Assynt and Gruinard blocks expose different levels of a once-contiguous crustal

202   fragment, and Love et al. (2004) to suggest that the Assynt and Gruinard blocks represent

203   discrete terranes.

204

205   *2.2. Post-Badcallian evolution and the relationship between the central and northern regions*

206

207   At the northern margin of the central region is the Laxford Shear Zone (LSZ), a

208   several kilometre wide WNW-trending, steeply south-dipping ductile shear zone involving

209   complex polyphase deformation and metamorphism that has been proposed to be an early

210   Proterozoic terrane boundary (Kinny and Friend, 1997; Friend and Kinny, 2001; Kinny et al.,

211   2005; Goodenough et al., 2010, 2013; Fig. 2). Within the LSZ and throughout the central

212   region, reworking of the granulite-facies gneisses is related to two separate post-Badcallian

213   tectonometamorphic events (Goodenough et al., 2010; Wheeler et al., 2010).

214   A series of steep NW–SE- to WNW–ESE-trending shear zones (Evans and Lambert,

215   1974; Coward and Park, 1987; Wheeler, 2007) is inferred to have developed during the

216   Inverian event (Evans 1965). Inverian metamorphism was associated with pervasive

217   retrogression of granulite facies assemblages, but only limited partial melting and

218   magmatism. These Inverian shear zones contain kinematic indicators consistent with

219   dominant bulk horizontal shortening (thrusting) with a small dextral component (Beach et al.,

220   1974; Coward and Park, 1987) that could explain juxtaposition of the central region

221   granulites over the lower-grade rocks of the northern region (Coward 1984, 1990; Wheeler et

222   al., 2010) and, furthermore, could have provided a potential source of the fluid required for

223   retrogression (Beach, 1980). *P–T* estimates for the Inverian event are 500–625 °C and 0.50–

224   0.65 GPa (Sills, 1983; Cartwright et al., 1985; Sills and Rollinson, 1987; Zirkler et al., 2012).

225   Pegmatites in the Lochinver and Scourie areas have been dated at *c*. 2.48 Ga (TIMS

226   U–Pb on zircon, Corfu et al., 1994; *in situ* SIMS Pb–Pb on monazite, Zhu et al., 1997).

227   Goodenough et al. (2013) report LA–ICPMS U–Pb ages from zircons within a folded and

228   foliated microgranite from Tarbet of 2.48 Ga and 1.76 Ga, which they interpret to date

229   metamorphism correlated with the Inverian and Laxfordian events (see below), respectively

230   (Fig. 3).

231   Inverian deformation and metamorphism was followed by emplacement of a suite of

232   mafic and ultramafic dykes (the Scourie Dykes; Peach et al., 1907; Sutton and Watson,

233   1951). Most of the dykes were intruded in the interval 2.42–2.37 Ga (U–Pb baddeleyite and

234   zircon ages, Davies and Heaman, 2014; Fig. 3) and are inferred to have been derived largely

235   from partial melting of metasomatically-enriched sub-continental mantle lithosphere (Hughes

236   et al., 2014). Hughes and co-workers suggest this enrichment may be related to subduction

237   during the late Archean.

238   Post-Scourie Dyke reworking associated with amphibolite facies metamorphism is

239   related to the late Paleoproterozoic Laxfordian event (Sutton and Watson, 1951; Goodenough

240   et al., 2010). In the central region, north of Scourie (Assynt block), retrogressed granulites are

241   cut by discrete metre-scale E–W-trending shear zones that deform and offset the Scourie

242   Dykes (Beach et al., 1974; Coward, 1990). These shear zones increase in abundance and

243   swing into a NW–SE orientation approaching the LSZ. Coward (1990) interpreted the large-

244   scale structures to indicate early Laxfordian dextral thrusting, although this deformation may

245   have been Inverian in age (Goodenough et al., 2010). Later sinistral extension (Beach et al.,

246   1974) was interpreted by Coward (1990) as due to Laxfordian reactivation of earlier

247   structures. Fluid ingress along amphibolite facies Laxfordian shear zones led to the

248   generation and intrusion of voluminous granite as dykes, and metasomatic alteration of both

249   Scourie Dykes and the TTG gneisses (Beach and Fyfe, 1972; Beach, 1973, 1976, 1980).

250   Zircons from a pre- to syn-Laxfordian granite from Ben Stack yielded an LA–ICP–

251 MS U–Pb age of 1.88 ± 0.2 Ga whereas those from an undeformed (post-Laxfordian) granitic

252 pegmatite from Badnabay gave an ID–TIMS U–Pb age of 1.77 ± 0.001 Ga (Goodenough et

253 al., 2013). A SHRIMP U–Pb zircon age of 1.854 ± 0.13 Ga was obtained from a composite

254 granite–pegmatite sheet just to the north of the LSZ (Friend and Kinny, 2001).

255

256 *2.3. Layered ultramafic–mafic bodies and metasedimentary rocks*

257

258   Layered ultramafic–mafic bodies, some several hundred metres in thickness, are

259 widely distributed across the central region, together constituting perhaps 5–10% of the total

260 outcrop (e.g. Peach et al., 1907; O'Hara 1961; Bowes et al., 1964; Davies, 1974; Sills et al.,

261 1982; Burton et al., 2000; Johnson et al., 2012; Fig. 2). Although generally sheet-like, the

262 larger layered bodies define open to isoclinal, upright to near-recumbent synforms (Davies,

263 1974; Cartwright et al., 1985), the cores of which are locally occupied by quartzo-feldspathic

264 garnet–biotite gneiss (hereafter brown gneiss; Sutton and Watson, 1951). In the literature

265 these brown gneisses have been interpreted as sedimentary in origin (e.g. Beach, 1974;

266 Cartwright et al., 1985; Cartwright and Barnicoat, 1987), but they could be volcanogenic

267 (discussed below); in either case, the spatial relationship suggests that the synforms are

268 synclines (Davies, 1974).

269   At their margins most of the ultramafic–mafic bodies are steeply inclined and appear

270 to be concordant with an intense steeply dipping fabric in the surrounding TTG gneisses that

271 is most intense at the contact with these bodies. These steeply dipping gneisses are

272 retrogressed to amphibolite facies, meaning that the marginal shear zones are Inverian (or

273 Laxfordian or a combination of both events) by definition (Evans, 1965), although the time at

274 which this steep fabric originally formed is uncertain.

12

275   The most extensive outcrops of layered ultramafic–mafic rocks and brown gneisses

276   occur in the north of the central region, towards the southern margin of the LSZ, where these

277   lithologies define a tightly folded belt up to a kilometre or more in width and extending for

278   more than 12 km along strike (Davies, 1974; Goodenough et al., 2010; Fig. 2). In addition,

279   layered ultramafic–mafic bodies crop out throughout the central region, particularly good

280   examples occurring on the flanks of Ben Strome (north-east of Kylesku) and close to the

281   villages of Scourie, Drumbeg and Achiltibuie (e.g. O'Hara, 1961; Bowes et al., 1964; Sills et

282   al., 1982; Johnson et al., 2012; Figs 1 and 2). Furthermore, smaller ultramafic and mafic

283   bodies are ubiquitous within the central region granulites, occurring as disrupted sheets and

284   pods several metres across down to centimetre-size remnants. The large ultramafic–mafic

285   bodies have major oxide, trace element and isotopic compositions suggesting they were

286   derived from MgO-rich (15–20 wt %) tholeiitic melts (Sills et al., 1982; Burton et al., 2000).

287   Mafic and ultramafic rocks have Sm–Nd whole rock ages of *c.* 3.0–2.7 Ga (e.g.

288   Whitehouse, 1989; Cohen et al., 1991; Whitehouse et al., 1996; Fig. 3); an age of 2.707 ±

289   0.052 Ga is interpreted as the time of igneous differentiation of the ultramafic–mafic bodies

290   (Cohen et al., 1991). Ultramafic–mafic rocks yield a Re–Os age of 2.686 ± 0.15 Ga (MSWD

291   = 1.43 and initial $^{187}Os/^{188}Os$=0.10940 ± 0.00076; Burton et al., 2000), interpreted by these

292   authors as the time of emplacement of the ultramafic–mafic bodies. However, there is

293   evidence for post-emplacement perturbation of both Sm–Nd and Re–Os isotopic systems

294   (Whitehouse et al., 1997; Burton et al., 2000). Zircon in a hornblendite from the Gruinard

295   block with a SIUMS U–Pb age of *c.* 2.8 Ga is interpreted to date metamorphism (Whitehouse

296   et al., 1997).

297   U–Pb zircon ages from samples of brown gneiss (LA-MC-ICP-MS and ID-TIMS,

298   Goodenough et al., 2013) and a rare white-mica gneiss (LA-MC-ICP-MS, Zirkler et al.,

299   2012) give a spread of ages along concordia from *c.* 2.8 to *c.* 2.5 Ga. Whether the data from

300   these putative metasedimentary rocks reflect detrital zircon grains older than c. 2.7 Ga and a

301   smear of metamorphic ages between two high-grade metamorphic events at *c.* 2.7 and *c.* 2.5

302   Ga, or a smear of detrital grains derived from protoliths older than 2.5 Ga followed by high

303   grade metamorphism at *c.* 2.5 Ga, is unclear. An in situ SIMS Pb–Pb age of 2526 ± 8 Ma

304   from a monazite included within garnet in an aluminous metasedimentary rock from north of

305   Scourie is interpreted by Zhu et al. (1997) to date a second granulite facies metamorphic

306   event.

307

308

309   **3. Field relations of the layered ultramafic–mafic bodies and metasedimentary rocks**

310

311   Notwithstanding that the large ultramafic–mafic bodies are bounded by steeply

312   dipping amphibolite facies shear zones, several of the bodies preserve pristine granulite facies

313   mineral assemblages in their core (O'Hara 1961, 1965; Johnson et al., 2012). While the

314   igneous origin of these bodies is not disputed, whether the commonly observed mineralogical

315   layering is a primary magmatic feature and whether apparent current and wedge cumulate

316   mineral 'bedding' reflect magma chamber processes have been matters of vigorous debate

317   (Bowes et al., 1964, 1966; O'Hara, 1965, 1966). Well exposed layered sequences of

318   ultramafic and mafic rocks occur near Scourie, Drumbeg, Achiltibuie and Ben Strome, as

319   well as in the southern part of the steeply dipping LSZ, in particular on Gorm Chnoc (Bowes

320   et al., 1964; Davies, 1974; Sills et al., 1982; Fig. 2).

321   Although there are local complexities and repetition of rock types that could be either

322   primary or due to post-emplacement deformation, the generalized sequence (Fig. 4a,b)

323   comprises metamorphosed layered ultramafic rocks (hornblende-bearing metapyroxenites

324   and metaperidotites mainly composed of assemblages of olivine, clinopyroxene,

14

325   orthopyroxene, hornblende, spinel and magnetite) at or near the base overlain by medium- to

326   coarse-grained hornblende-bearing two-pyroxene mafic rocks (mainly composed of

327   assemblages of plagioclase, clinopyroxene, hornblende and orthopyroxene with or without

328   garnet). In some instances the mafic rocks may be subdivided into a coarse-grained,

329   plagioclase-deficient but garnet-rich lower unit overlain by a medium- to coarse-grained

330   upper unit containing little or no garnet but a higher proportion of plagioclase. Where such a

331   relationship exists, the change from one variant to the other is gradational. In some examples,

332   felsic layers near the top of the sequence have been termed anorthosite and interpreted as

333   primary, produced by fractionation of the mafic magmas (Bowes et al., 1964; Davies, 1974).

334   In other cases, these felsic layers have been interpreted as intrusive (Weaver and Tarney,

335   1980), corresponding to crystallised melt derived from anatexis of the metabasic rocks

336   (Johnson et al., 2012).

337   Individual ultramafic–mafic bodies commonly preserve only a portion of the

338   succession described above, in many cases due to subsequent faulting/shearing. However, in

339   all of the larger layered bodies mafic rocks are dominant. Although ultramafic rocks may

340   constitute up to a third of some bodies by area (e.g. in the body near Drumbeg; Fig.1; Bowes

341   et al., 1964), in many cases ultramafic rocks are absent.

342   Where exposed, brown gneisses commonly occur within synclinal cores of the larger

343   ultramafic–mafic bodies at the highest structural levels, although similar lithologies may

344   occur as highly strained units enclosed within the felsic orthogneisses. The most extensive

345   exposures of brown gneiss occur in the southern part of the LSZ (Davies, 1974; Fig. 2), in the

346   core of the Cnoc an t'Sidhean body SE of Stoer (Cartwright et al., 1985; Cartwright and

347   Barnicoat 1986; Zirkler et al., 2012; Fig. 1) and around 1 km NNW of Scourie (Beach, 1974;

348   Zhu et al., 1997; Fig. 1 and 2). The brown gneisses contain garnet, biotite and/or hornblende,

349   plagioclase, quartz and accessory minerals, in which the proportion of mafic to felsic

15

350   minerals varies widely. They range in composition from hornblende-rich metaluminous

351   variants to peraluminous biotite-rich sillimanite- and kyanite-bearing gneisses that lack

352   hornblende. In situ partial melting and two phases of garnet growth suggest the brown

353   gneisses were metamorphosed to granulite facies then experienced extensive amphibolite

354   facies (probably Inverian) retrogression (Zirkler et al., 2012).

355   Steeply-inclined shear zones at the margins of the ultramafic–mafic bodies in the

356   southern part of the LSZ are characterised by amphibolite-facies mineral assemblages and a

357   strong S- to SE-plunging stretching lineation which, in appropriate rocks, is defined by

358   elongate garnet porphyroblasts, attesting to intense post-Badcallian deformation. In close

359   proximity to the ultramafic–mafic bodies, the TTG gneisses are also strongly retrogressed,

360   comprising assemblages including plagioclase, quartz, green hornblende, biotite and epidote.

361

362

363   **4. Geochemistry**

364

365   Major and trace element concentrations were determined for 29 metabasic rocks

366   (from Johnson et al., 2012), 14 ultramafic rocks, 17 brown gneisses (from Zirkler et al., 2012

367   and new data; only 9 samples analysed for trace elements), 12 felsic sheets interpreted to

368   have been derived from partial melting of the metabasic rocks (from Johnson et al., 2012),

369   and 17 retrogressed (hornblende- and/or biotite-bearing) TTG gneisses collected from within

370   50 metres of a large ultramafic–mafic body. The metabasic rocks are subdivided into those

371   that contain little or no garnet (n=14; hereafter garnet-poor metabasic rocks) and those that

372   contain abundant garnet (n=15; hereafter garnet-rich metabasic rocks). Analytical procedures

373   follow Johnson et al. (2012) and Zirkler et al. (2012). The full geochemical dataset is

374   available in the Supplementary Data.

375   Included for comparison in the figures and discussion below are the compositions of

376   (i) komatiites (n > 200) from greenstone belts within the Superior Province and North

377   Atlantic craton using appropriate analyses from the GEOROC database (http://georoc.mpch-

378   mainz.gwdg.de/); (ii) Archean (meta)basalts (n = 72) from greenstone belts from the Superior

379   and North Atlantic cratons [hereafter SNAC basalts; data from Kerrich et al. (1999) – Mg- to

380   Fe-tholeiitic basalts from the Superior Province; Polat (2009) – tholeiitic and transitional

381   alkaline basalts from the Superior Province; Ordóñez-Calderón et al. (2011) – mafic

382   amphibolites from SW Greenland interpreted as metamorphosed basalts produced in a

383   subduction environment]; (iii) the major element compositions of 14 Archean non-arc basalts

384   considered to represent near-primary partial melts of fertile mantle sample KR–4003

385   (Walther, 1998; Herzberg et al., 2010); (iv) the composition of mid ocean ridge basalt

386   (MORB) according to Hofmann (1988) and Sun and McDonough (1989), the latter of which

387   has a major element composition that is practically indistinguishable from the mean

388   composition of 'ALL MORB' determined by Gale et al. (2013); and, (v) garnet–biotite

389   gneisses from the Storø greenstone belt, SW Greenland (Ordóñez-Calderón et al., 2011) that

390   are petrographically similar to the brown gneisses. Also shown are the mean compositions of

391   olivine (ol) and clinopyroxene (cu) from a typical metamorphosed ultramafic rock (SC03)

392   and clinopyroxene (cm) from a typical garnetiferous mafic rock (SC01) as measured by

393   EPMA (Johnson and White, 2011; unpublished data). Both these samples are from near

394   Scourie in the Assynt block (Fig. 1).

395

396   *4.1. Major oxides*

397   Figure 5 shows the concentration of selected major oxides and X_{Mg} [molar

398   MgO/(MgO/FeO)] plotted against MgO (wt%), on which the average compositions of all

399   mafic rocks, metamorphosed ultramafic rocks and the Archean non-arc basalts are shown for

400   reference. The metamorphosed ultramafic rocks contain 41–50 wt% SiO_2 and 32–19 wt%

401   MgO, and have X_{Mg} of 0.76–0.84. A linear trend is evident for most oxides that projects close

402   to the mean composition of olivine in the ultramafic sample SC03 at its high MgO end and

403   close to the average composition of the Archean non-arc basalts at its low MgO end. SiO_2,

404   TiO_2, Al_2O_3, CaO, Na_2O and MnO (not shown) are all negatively correlated against MgO

405   (Fig. 5). The average composition of the ultramafic rocks is similar to the most MgO-rich of

406   the Archean non-arc basalts, which together define a compositional trend for several oxides

407   (SiO_2, Al_2O_3, FeO and CaO) when plotted against MgO that is considered to be a function of

408   the temperature and degree of partial melting of the mantle, both of which increase with

409   increasing MgO (e.g. Herzberg et al., 2010; Johnson et al., 2014).

410   All analysed mafic rocks are olivine normative (6–20 vol.%) except three garnet-poor

411   samples that contain minor (<2.5 vol.%) normative quartz. Although there is considerable

412   compositional spread and overlap, and few clear compositional trends, the variation diagrams

413   show that the garnet-poor and garnet-rich metabasic rocks exhibit some compositional

414   differences. In general, garnet-poor samples have higher SiO_2 and Na_2O and lower FeO and

415   Al_2O_3 contents compared to garnet-rich samples (Fig. 5; Johnson et al., 2012). A weak linear

416   trend evident in the plot of MgO vs Al_2O_3, defined largely by the garnet-rich metabasic rocks,

417   extends towards the average compositions of clinopyroxene at its low Al_2O_3, high MgO end.

418   The overall compositional range of the mafic rocks is similar to the SNAC basalts, although

419   several are relatively depleted in SiO_2, Na_2O, TiO_2 and K_2O and slightly enriched in MgO,

420   CaO and possibly FeO. The X_{Mg} of the metabasic rocks varies widely from 0.34–0.74, similar

421   to that recorded by the SNAC basalts. Compared to MORB, the average of all mafic rocks

422   contains similar concentrations of MgO, CaO and Al_2O_3, but is moderately to strongly

423   depleted in Na_2O, TiO_2 and SiO_2 and slightly enriched in K_2O.

424   The brown gneisses have major oxide compositions that are generally

425   indistinguishable from those of the retrogressed TTG gneisses and felsic sheets, although

426   some samples are relatively enriched in FeO and MnO (not shown) and depleted in Na_2O.

427   The brown gneisses, TTG gneisses and felsic sheets together define a linear trend for many of

428   the major oxides (excluding TiO_2) that broadly projects towards the average of the mafic

429   rocks and MORB at higher MgO and lower SiO_2, although there is significant scatter in

430   Al_2O_3, Na_2O and K_2O.

431   Figure 6a shows the composition of the ultramafic and mafic rocks plotted on an

432   AFM diagram (A = Na_2O + K_2O; F = total Fe expressed as FeO; M = MgO). Most have low

433   total alkali contents and define a trend of strong enrichment in Fe that is characteristic of

434   tholeiitic magmas. Although it is unclear which, if any, of the rocks are volcanic, Fig. 6b

435   shows the compositions of the metabasic rocks and brown gneisses plotted on the total alkalis

436   versus silica (TAS) diagram (Le Maitre et al., 2002). The mafic rocks generally lie within the

437   basalt field, with four of the garnet-rich and one of the garnet-poor samples plotting within

438   the picrobasalt field, and two of the garnet-poor samples within the basaltic andesite field. In

439   the TAS diagram, the brown gneisses plot across a range of fields from basalt to rhyolite,

440   with most plotting in the fields of andesite and dacite (Fig. 6b).

441

442   *4.2. Trace elements*

443

444   The primitive mantle normalised trace element compositions of the main rock types

445   are shown in Fig. 7 in which elements are ordered from left to right by increasing

446   compatibility in oceanic basalts (Hofmann, 1988). Data for the felsic sheets are given in

447   Johnson et al. (2012).

448   The ultramafic rocks mostly have flat patterns for the more compatible trace elements

449   with concentrations that are around 1–3 times primitive mantle values (Fig. 7a). All samples

450   contain concentrations of Cs and Rb that are around an order of magnitude higher than

451   primitive mantle; K and light rare earth element (LREE) contents are highly variable. A small

452   negative Ti anomaly is evident and several samples have concentrations of Nb and Ta similar

453   to, or below, primitive mantle values.

454   Relative to SNAC basalts and MORB (light and dark grey fields in Fig. 7c and d,

455   respectively), almost all metabasic rocks (those with high P_2O_5 contents are excluded;

456   Johnson et al., 2012) are weakly to strongly depleted in Hf, Zr and Ti, and several of the

457   garnet-poor samples and many of the garnet-rich samples are moderately to strongly depleted

458   in Th, U, Nb and Ta (Fig. 7b,c). All mafic rocks show highly variable LILE concentrations

459   (Cs, Rb, Ba, K) that are elevated relative to MORB but similar to the range recorded by

460   SNAC basalts (Fig. 7b,c).

461   The brown gneisses (Fig. 7d) have trace element compositions similar to the

462   retrogressed TTG gneisses (Fig. 7e), although the former show greater variation in Hf and Zr,

463   less variation in heavy rare earth element (HREE) contents and are marginally less depleted

464   in Ti. Relative to petrographically similar garnet–biotite gneisses from the Storø greenstone

465   belt, SW Greenland (Ordóñez-Calderón et al., 2011; grey field in Fig. 7d), a majority of

466   brown gneiss samples are depleted in Cs, Rb, Th, U, Nb, Ta and Zr but enriched in Sr. Felsic

467   sheets within the ultramafic–mafic bodies have trace element compositions similar to

468   proximal TTG gneisses, although many show some relative depletion in Nb, Ta, Ti and Y

469   (Johnson et al., 2012).

470   Figure 4c shows REE abundances normalised to CI chondrite of McDonough and Sun

471   (1995), in which the plots are arranged in the simplified stratigraphic order described

472   previously. Ultramafic rocks have REE abundances ≤ 10 times chondrite values (cf. Sills et

473   al., 1982) and flat patterns in which $(La/Lu)_N = 1–2$, except three samples with higher LREE

474   concentrations and moderately fractionated patterns (Fig. 4c).

475   Garnet-rich mafic rocks have significantly lower LREE concentrations than garnet-

476   poor variants (Fig. 4c). Several garnet-rich samples are LREE depleted $[(La/Sm)_N <1]$ with

477   flat middle to heavy REE patterns, others have $(La/Lu)_N > 1$ (Johnson et al., 2012). A small

478   positive Eu anomaly (Eu/Eu* up to 1.5) occurs in three samples. In comparison, garnet-poor

479   mafic rocks have a wider range of REE abundances. Although all samples have flat middle to

480   heavy REE patterns, there are two compositional groups apparent, one with flat LREE

481   patterns and another showing pronounced LREE enrichment $[(La/Sm)_N$ up to 3.5; Fig. 4c].

482   Both small positive and negative Eu anomalies occur (Eu/Eu* = 0.6–1.4), although the

483   majority are negative (Johnson et al., 2012).

484   The retrogressed host TTG gneisses have steep REE patterns [mean $(La/Lu)_N$ of 41]

485   and exhibit pronounced LREE enrichment with $(La/Sm)_N$ of 3–8. Most samples show a

486   positive Eu anomaly in which the magnitude of Eu/Eu* (up to 2.8) is inversely correlated

487   with overall REE abundance. The brown gneisses have moderately fractionated REE patterns

488     $[(La/Lu)_N = 2–42]$ and a relative enrichment of LREE to HREE, in which $(La/Sm)_N = 2.5–6.3$

489   and $(Gd/Lu)_N = 1.0–3.8$. Samples exhibit small Eu anomalies that are both positive and

490   negative (Eu/Eu* = 0.8–1.8). The concentration of HREE in the brown gneisses is similar to

491   the metabasic rocks and, in general, significantly higher than in the TTG gneisses.

492

493

494   **5. Discussion**

495

496   Within the central region of the mainland Lewisian Complex, the rocks record

497   evidence of polyphase deformation and at least three phases of granulite to amphibolite facies

21

498   metamorphism, including partial melting of most rocks, during a tectono-metamorphic

499   evolution spanning around a billion years. The field relationships and igneous, structural,

500   metamorphic and geochemical (including isotopic) information preserved in the rocks reflect

501   this complicated, long-lived high-temperature tectonic evolution. As a result, the early (pre-

502   Badcallian to Badcallian) structural evolution is difficult or impossible to unravel and the

503   compositional data as it pertains to the origin and early evolution of the rocks is ambiguous.

504   Such a situation is not unique to the Lewisian Complex, but is a common feature of Archean

505   high-grade grey gneiss terrains (e.g. West Greenland, Nutman et al., 2013, 2015), leading to

506   inherent ambiguity in constraining the geodynamic regime responsible for the origin of these

507   terrains.

508

509   *5.1. The nature of the protoliths*

510

511   *5.1.1.Major oxide compositions*

512   Sills et al. (1982) proposed that the composition of the ultramafic and mafic rocks

513   could be explained by fractionation via crystal settling of dominantly olivine and pyroxene

514   from a high MgO 'komatiitic' mantle-derived (tholeiitic) melt, a conclusion supported by the

515   whole rock major oxide data presented here. Plotted against MgO content, the

516   metamorphosed ultramafic rocks define a broad trend between the average composition of

517   olivine from a typical metamorphosed ultramafic rock and the average composition of

518   Archean non-arc basalts (Fig. 5). The mafic rocks show considerable scatter for the major

519   oxides. This likely reflects a complex combination of igneous processes (mainly olivine- and

520   clinopyroxene-dominated fractional crystallisation of the primary magmas), and high-grade

521   metamorphic processes (partial melting and melt loss from the mafic rocks, and possible

522   contamination by TTG host rocks and melts derived therefrom; Johnson et al., 2012, 2013).

523   Notwithstanding, the average compositions of the metamorphosed ultramafic rocks, the mafic

524   rocks and the Archean non-arc basalts define a broadly co-linear trend for all major oxides,

525   except SiO_2 and Na_2O (see below). This relationship suggests a possible genetic link between

526   the ultramafic rocks, mafic rocks and a magma similar in composition to an average of the

527   Archean non-arc basalts. On this basis we propose that the metamorphosed ultramafic rocks

528   could represent the earliest cumulate material whereas the evolving melt could have

529   fractionated to form the range of mafic compositions (cf. Sills et al., 1982).

530   Most ultramafic and mafic rocks contain brown (Ti-rich) hornblende interpreted to

531   have been stable at the metamorphic peak (Johnson et al., 2012). This indicates that these

532   rocks were hydrated prior to granulite facies metamorphism. Whether the primary magmas

533   from which these rocks crystallised were hydrated, or whether the H_2O was introduced

534   subsequently, is uncertain. However, the observation that brown hornblende is apparently

535   evenly distributed throughout the ultramafic–mafic rocks rather than developed only at the

536   margins of the large ultramafic–mafic bodies and/or along planar structures that might record

537   channelized fluid influx, suggests the primary magmas may have been hydrous and were

538   derived from a hydrated mantle source.

539   The marked depletion in TiO_2 in the rocks relative to primitive mantle compositions

540   (Fig. 7) likely reflects characteristics of the mantle source. However, the overall enrichment

541   of the garnet-poor mafic rocks in SiO_2 and Na_2O and depletion in Al_2O_3 relative to the

542   garnet-rich samples may suggest that the latter comprise a higher proportion of the cumulate

543   and retained less trapped melt than the former prior to solidification. This interpretation is

544   consistent with the simplified stratigraphic sequence shown in Fig. 4a. Although we follow

545   Sills et al. (1982) and Johnson et al. (2012) in interpreting most of the mafic rocks as

546   metamorphosed intrusive rocks (i.e. metagabbros), is it possible that some of the garnet-poor

547   mafic rocks, particularly those occurring near the structural tops of the large ultramafic–mafic

548   bodies, were extrusive (i.e. metabasalt).

549   Concentrations of SiO_2, Na_2O and K_2O in the mafic rocks are on average depleted

550   relative to SNAC basalts, as illustrated in Fig. 8. This feature conforms to a general model of

551   partial melting of amphibolite whereby the mafic rocks are residual after extraction of melt,

552   in which melt compositions are consistent with the felsic sheets (Johnson et al., 2012; Fig. 5).

553   Depletion of SiO_2 and Na_2O by melting of the metabasic rocks explains the nonconformity of

554   these major oxides with the fractionation trend discussed above.

555

556   *5.1.2. Trace element compositions*

557   During the past forty years geochemical methods have been developed to enable

558   discrimination among tectonically defined magma types for volcanic rocks, in particular

559   basalts (e.g. Pearce and Cann, 1973; Pearce and Peate, 1995; Pearce, 2008). Such

560   discrimination has proven particularly useful where the magma source cannot be

561   unambiguously deduced using other methods, for example in the case of ophiolites (Pearce,

562   2008, 2014b). However, the ability to correctly discriminate samples from mid-ocean ridges,

563   island arcs and ocean islands using binary and ternary diagrams has been assessed as no

564   better than 60% (Snow, 2006), and the use of these diagrams at all in discrimination of

565   magma type has been challenged (Li et al., 2015). This calls into question whether such

566   diagrams should be used in assessing the tectonic setting of Archean greenstones (Pearce,

567   2008; Condie, 2015).

568   In this study it is unclear which, if any, of the samples might have had the volcanic

569   protoliths that are generally required for geochemical discrimination of magma type.

570   Furthermore, the extent to which trace element data may be used to elucidate tectonic

571   environments in rocks that have undergone strong modification by magmatic and

572   metamorphic fractionation, as well as probable contamination with their host rocks, is

24

573 questionable (Pearce, 2008, 2014a; Rollinson and Gravestock, 2012). Although many trace

574 elements may be considered immobile during high-temperature subsolidus metamorphism

575 and hydrothermal alteration, most have mineral/melt distribution coefficients that are far

576 from unity, leading to significant modification of trace element compositions as a result of

577 crystal settling and/or partial melting and melt loss (Fig. 8). Notwithstanding, the trace

578 element compositions may be useful in interpreting some aspects of source characteristics

579 (Condie, 2015).

580 The brown gneisses show significant depletion in most LILE compared to

581 petrographically similar garnet–biotite gneisses from SW Greenland (Ordóñez-Calderón et

582 al., 2011; Fig. 7a), consistent with partial melting and melt loss (Cartwright and Barnicoat,

583 1987; Zirkler et al., 2012). The trace element composition of the brown gneisses is broadly

584 similar to that of the TTG gneisses (Fig. 7), except for the HREE contents, which are similar

585 to the mafic rocks but mostly higher than in the TTG gneisses (Fig. 4c). This indicates that

586 the brown gneisses cannot have been formed solely from the TTG gneisses.

587 For the garnet–biotite gneisses and associated quartz-rich rocks from southern West

588 Greenland, the petrogenetic interpretation preferred by Ordóñez-Calderón et al. (2011) is that

589 some represent metamorphosed altered basaltic rocks (greenstones) whereas the bulk are

590 metamorphosed siliciclastic rocks derived by erosion of a mixture of felsic and mafic igneous

591 rocks. However, these authors acknowledge ambiguity in their interpretation. The brown

592 gneisses in the central region of the Lewisian complex are similarly enigmatic. Their

593 protoliths could conceivably have been: (i) sedimentary rocks derived by erosion of both the

594 TTG-dominated crust and associated ultramafic–mafic complexes prior to the granulite facies

595 metamorphism; (ii) erupted (volcanic) equivalents of the mafic to felsic plutonic rocks; (iii)

596 orthogneisses metasomatised during the prograde granulite facies metamorphism; or (iv) one

597 or more combinations of the origins suggested in (i) to (iii). Based on the general spatial and

598   stratigraphic distribution of the brown gneisses (Fig. 2) and the rounded nature of the zircons

599   (Zirkler et al., 2012; Goodenough et al., 2013), the interpretation preferred here is that most

600   of the brown gneisses represent metamorphosed sedimentary or volcano-sedimentary rocks.

601   Accepting the caveats discussed above concerning binary discrimination diagrams,

602   the composition of the brown gneisses is compared with similar rocks from southern West

603   Greenland, and the mafic rocks (which may or may not approximate liquid compositions)

604   with the SNAC basalts on three popular discrimination diagrams (Fig. 9). On the Ti/Y vs

605   Nb/Y diagram the brown gneisses plot in fields ranging from basalt to rhyolite/dacite, similar

606   to the garnet–biotite gneisses from Greenland (Fig. 9a), whereas most of the mafic rocks plot

607   within the basalt field, with the remainder plotting within the basaltic andesite/andesite field

608   at higher Ti. Excluding those non-basaltic samples (i.e. those with $SiO_2 > 60$ wt%), on the

609   Th/Yb vs Nb/Yb diagram (Fig. 9b) the brown gneisses are scattered, with three of the four

610   samples plotting close to or below the MORB–ocean island basalt (OIB) array. By contrast,

611   the Greenland samples plot in the field of continental arc rocks above the MORB–OIB array

612   at high Nb/Yb (Pearce, 2008). The mafic rocks show no coherent trend in Fig. 9b; several

613   samples plot below the MORB–OIB array, consistent with partial melting and melt loss. On

614   the Nb/Y vs TiO_2/Yb diagram (Fig. 9c) the four low-silica brown gneisses lie in or below the

615   MORB array, with three plotting close to the composition of E–MORB, although this proxy

616   is not considered effective for fingerprinting Archean tectonic settings (Pearce 2008). Most of

617   the mafic rocks also plot in the MORB array and many plot close to the composition of N–

618   MORB.

619   A pronounced depletion in Nb, Ta and Ti is a characteristic geochemical signature of

620   rocks from the Lewisian Complex (Fowler, 1986; Rollinson, 1996) and is seen in all samples

621   in this study (Fig. 7). Several of the ultramafic rocks have concentrations of Nb and Ta that

622   are lower than primitive mantle values (Fig. 7a), the mafic rocks are depleted relative to

623   SNAC basalts and MORB (Fig. 7b,c; Fig. 8; Johnson et al., 2012), the brown gneisses are

624   depleted relative to similar rocks in Greenland (Fig. 7d) and the proximal TTG gneisses (Fig.

625   7e; discussed in detail below). This 'arc-like' signature may be interpreted to reflect the

626   presence of rutile in the source rocks at depth, a feature that is commonly invoked to indicate

627   formation in a subduction environment (e.g. Moyen, 2011).

628   Central region TTG gneisses have the high SiO_2, Na/K, Sr/Y and depleted HREE

629   signatures that characterise most sodic Archean TTGs worldwide, consistent with an

630   interpretation that most TTGs equilibrated with a garnet- and clinopyroxene-bearing (with or

631   without hornblende) residue that lacked plagioclase (Moyen, 2011). Moreover, TTG gneisses

632   from the central region show a pronounced depletion in Ta, Nb and Ti relative to an average

633   sodic TTG composition (Johnson et al., 2013, fig. 2), suggesting their source rocks also

634   contained rutile. A common hypothesis is the TTG gneisses formed by partial melting of

635   garnet- and rutile-bearing amphibolites or eclogites in a subducting slab (e.g. Drummand and

636   Defant, 1990; Martin, 1999; Rapp et al., 2003). However, the presence of garnet- and rutile-

637   bearing residual source rocks that exhausted plagioclase does not necessarily mean that those

638   source rocks were eclogites or that the source rocks were stable at eclogite facies pressures

639   (e.g. Johnson et al., 2014). Both experiments (Qian and Hermann, 2013; Zhang et al., 2013)

640   and phase equilibria modelling (Johnson et al., 2014) show that suitable garnet- and rutile-

641   bearing residues can be produced at pressures of 1.5 GPa or less. In addition, geochemical

642   and experimental data suggest that most TTGs, including those from the Lewisian Complex,

643   were derived from a LILE-enriched source similar to oceanic plateau basalts, and are unlikely

644   to have been derived from anatexis of MORB in a subduction zone setting (Martin et al.,

645   2014).

646   Negative anomalies in Nb, Ta and Ti as well as an enrichment in Th, LREE and other

647   LILE are recorded in younger (Palaeoproterozoic) rocks of the Scourie Dyke swarm and

27

648   mantle xenoliths that sample the sub-continental mantle lithosphere underlying the Lewisian

649   Complex (Hughes et al., 2014). Trace element modelling led Hughes and co-workers to

650   conclude that the sub-continental mantle lithosphere was metasomatised by devolatilisation

651   of a subducting slab during the Archean and/or had interacted with carbonatitic melts.

652   Although subduction is one way of getting hydrated material into the mantle, it is not the only

653   plausible mechanism. Bédard (2006) suggested that TTG magmas may be generated at the

654   base of thick plateau-like units of hydrated basaltic crust. In his model, the dense garnet- and

655   hornblende-bearing residues delaminated, refertilising the sub-continental mantle lithosphere

656   and triggering additional melting (see also Bédard et al., 2003, 2013). Geodynamic models

657   that consider higher mantle temperatures appropriate to the Archean and incorporate

658   calculated phase equilibria and experimentally determined melting relations have

659   demonstrated the plausibility of this alternative mechanism of mantle refertilisation (Johnson

660   et al., 2014; Sizova et al., 2015). In summary, similar to other regions, the trace element

661   composition of rocks from the central region of the Lewisian Complex does not allow

662   unambiguous discrimination of the tectonic setting in which the rocks formed (cf. Pearce,

663   2014a).

664

665   *5.2. Field and metamorphic evidence*

666

667   Large kilometre- to decametre-scale layered ultramafic–mafic bodies within the

668   central region of the Lewisian Complex are distinct from smaller ultramafic and mafic sheet-

669   like and podiform bodies that are ubiquitous at outcrop scale throughout the central region.

670   The difference is not just in scale (the layered bodies are larger by an order of magnitude or

671   more), but also in the fact that many of the metabasic rocks in the layered bodies contain

28

672   abundant garnet, whereas the smaller sheet-like bodies do not. Nonetheless, the large

673   ultramafic–mafic bodies could be genetically related to these smaller bodies.

674   Based on field evidence from Badcall (Fig. 1), Rollinson and Windley (1980)

675   suggested that the TTG gneisses intruded, and therefore post-dated, the layered ultramafic–

676   mafic bodies (their figure 1), an interpretation followed by Rollinson and Gravestock (2012).

677   During the course of this work we have found no convincing evidence in the field, at Badcall

678   or elsewhere, to support this interpretation (although the mafic rocks are commonly cross-cut

679   by bodies of tonalite–trondhjemite derived from partial melting of the mafic rocks and TTG

680   gneisses; Johnson et al., 2010). In addition, this relative age relationship contradicts the

681   isotopic age data, much of which suggests that the TTG gneisses are older than the mafic–

682   ultramafic rocks (Whitehouse, 1989; Cohen et al., 1991; Friend and Kinny, 1995;

683   Whitehouse et al., 1996; Kinny and Friend, 1997; Burton et al., 2000; Fig. 3).

684   The large layered ultramafic–mafic bodies are bounded by steeply dipping shear

685   zones. Furthermore, some of these bodies are spatially associated with brown gneisses of

686   probable supracrustal origin. The folded and disrupted belt of layered ultramafic–mafic

687   bodies and brown gneisses in the south of the LSZ shows a broadly symmetrical distribution

688   of rock types (Fig. 2). If this belt represents lateral accretion due to closure of an ocean basin

689   via asymmetric (one-sided) subduction, then the metamorphosed equivalents of other

690   lithologies typically associated with active margins (e.g. ophiolites, mélanges/olistostromes,

691   cherts, banded iron formations (BIF), black shales, carbonate rocks, etc.), are notably lacking

692   in the central region. Although such lithological associations diagnostic of subduction–

693   accretion do occur in the mainland Lewisian Complex, forming the Loch Maree Group

694   within the southern region (Park et al., 2001), these protoliths are significantly younger (c.

695   2.0 Ga; O'Nions et al., 1983; Whitehouse et al. 1997) than those in the central region, and

696   record Paleoproterozoic, not Archean, processes (Park et al., 2001; Mason, 2015).

697　　　　Assuming the brown gneisses represent supracrustal rocks, the spatial relationship

698　　between the brown gneisses and several ultramafic–mafic bodies requires burial of these

699　　lithologies from the near surface to depths exceeding 25 km prior to or during granulite facies

700　　metamorphism. Folding of the ultramafic–mafic belts and associated supracrustal rocks is

701　　considered by Davies (1976) to have occurred during the Archean prior to the peak of

702　　Badcallian metamorphism. Thus, the geometry of both the belt of ultramafic–mafic bodies

703　　and supracrustal rocks in the southern LSZ, as well as more isolated ultramafic–mafic bodies,

704　　could be interpreted in terms of pre- to syn-Badcallian gravity-driven sinking (sagduction) of

705　　the dense ultramafic–mafic bodies (and structurally-overlying supracrustal rocks) into the

706　　underlying less dense and less viscous partially molten TTG gneisses (cf. Anhaeusser, 1975;

707　　Brun, 1980; Brun et al., 1981; Ramsay, 1989; Bouhallier et al., 1995; Kisters & Anhaeusser,

708　　1995; Chardon et al., 1996, 1998; Collins et al., 1998; Bremond d'Ars et al., 1999; Marshak,

709　　1999; Wellman, 2000; Sandiford et al., 2004; Van Kranendonk et al., 2004, 2014; Parmenter

710　　et al., 2006; Robin and Bailey 2009; Thebaud and Rey 2013; François et al., 2014; Sizova et

711　　al., 2015).

712　　　　Based on mineral equilibria modelling, there is no evidence that the ultramafic–mafic

713　　rocks reached pressures significantly higher than the inferred Badcallian metamorphic peak

714　　(Johnson and White, 2011). The implied clockwise *P–T* path, in which peak *T* and *P* coincide

715　　(Johnson & White, 2011, fig. 5b), is similar to those modelled for Archean sagduction

716　　(Francois et al., 2014), the results of which suggest the process is rapid and occurs within a

717　　few million years. The apparent thermal gradient of ~925 ºC/GPa lies within the range for

718　　Precambrian granulite–ultrahigh temperature metamorphism (750–1500 ºC/GPa) but well

719　　above that for Precambrian eclogite–high pressure granulite metamorphism (350–750

720　　ºC/GPa) that has been interpreted to record the start of Archean subduction (Brown, 2014).

721　　Furthermore, Phanerozoic subduction–accretion is associated with more hairpin-like

722 clockwise *P–T* paths in which the pressure peak coincided with or preceded the temperature

723 peak (e.g. Liou et al, 2014). There is no evidence for regional blueschist or eclogite facies

724 metamorphism in the central region that is a signature of late Neoproterozoic and

725 Phanerozoic subduction. If it is confirmed that fragments of garnet pyroxenite in the

726 ultramafic–mafic bodies reached eclogite facies, as reported by Sajeev et al. (2013), an origin

727 as entrained deep-seated remnants of delaminating lower crust is a plausible explanation

728 (Sizova et al., 2015).

729 Although primary (early) structural relationships have been destroyed by the intense

730 polyphase ductile deformation, some of the smaller metre- to centimetre-scale ultramafic and

731 mafic sheet-like bodies that are ubiquitous within the central region could represent disrupted

732 dykes through which the original greenstone belt magmas were supplied from depth. Also,

733 the geochemistry of these smaller bodies is likely to reflect interaction with the suprasolidus

734 (melt-bearing) host TTG gneisses, as suggested by the variable REE chemistry of

735 clinopyroxene from ultramafic rocks preserved at different scales (Rollinson and Gravestock,

736 2012).

737 Sinking of the large layered ultramafic–mafic bodies and associated supracrustal

738 rocks during the Archean prior to or synchronous with Badcallian granulite facies

739 metamorphism would have given rise to structures with steeply dipping foliations and

740 lineations at their margins (Collins et al., 1998; Marshak, 1999; Van Kranendonk et al., 2004;

741 Parmenter et al., 2006; Lin and Beakhouse, 2013; Thébaud and Rey, 2013), perhaps

742 consistent with the initial (pre- to syn-Badcallian) development of the shear zones that occur

743 at the margins of these bodies. However, subsequently these structures would have acted as

744 strong foci for deformation and fluid flow, in agreement with the strong localisation of strain

745 and retrogression during the subsequent Inverian and Laxfordian events, which caused

746 extensive overprinting of pre- to syn-granulite facies deformation and mineral assemblages.

747 A strong S- to SE-plunging stretching lineation defined by garnet is common at the margins

748 of the large ultramafic–mafic bodies, attesting to intense post-Badcallian deformation of

749 these bodies. Despite the fact that unambiguous evidence is absent due to successive

750 overprinting deformations, the shear zones spatially associated with the ultramafic–mafic

751 bodies may represent early (Badcallian) structures that were subsequently reactivated by

752 Inverian and Laxfordian deformation.

753   Although the fundamental driving force for sagduction of greenstone belts is the

754 negative buoyancy of the denser ultramafic and mafic rocks ($\rho > 3.0$ gcm^{-3}) relative to

755 underlying felsic orthogneisses ($\rho \sim 2.7$ gcm^{-3}), it is thermal weakening of the basement and a

756 low viscosity in the immediately underlying mantle that control the process (Sandiford et al.,

757 2004; Thebaud and Rey 2013; Johnson et al., 2014). The dynamic requirements for

758 sagduction were evidently met in many greenstone belts (Anhaeusser 1975; Brun 1980; Brun

759 et al., 1981; Bouhallier et al., 1995; Chardon et al., 1996, 1998; Collins et al., 1998;

760 Parmenter et al., 2006; Robin and Bailey 2009; Wellman, 2000) and sagduction plausibly

761 could have occurred in the central region of the Lewisian Complex, particularly as the

762 basement rocks at depth were at temperatures in excess of 900 °C and partially molten

763 (Johnson et al., 2013).

764   The ultramafic–mafic bodies could conceivably represent the metamorphosed

765 equivalents of: accreted oceanic crust, lower crustal underplates, a single disrupted large

766 layered intrusion emplaced into felsic crust, multiple layered intrusions of a similar age,

767 multiple layered intrusions of variable age, differentiated intrusions near the base of a

768 greenstone belt, or interlayered komatiitic and basaltic lava flows near the base of a

769 greenstone belt. The brown gneisses may represent (volcano) sedimentary rocks from higher

770 crustal levels. If the rocks do represent the sunken remnants of dense upper crust, at some

771 point the downward motion of the greenstone belts was arrested. Why would this have

772 happened?

773   The ultramafic–mafic bodies, metasedimentary rocks and host TTG gneisses record

774 similar peak T and P conditions (Johnson and White 2011; Zirkler et al., 2012; Johnson et al.,

775 2013), which implies they were present together in the deep crust close to the Badcallian

776 metamorphic peak. One possible explanation for the arrested downward flow of the

777 greenstones is stiffening of the crust at depth. If prograde melt production and drainage from

778 the fertile TTGs ceased during sagduction of the greenstones as the metamorphic peak was

779 approached and as heat flow declined, the residual TTG crust could have become

780 significantly more viscous halting the sinking greenstones.

781   The dynamic plausibility of these processes requires evaluation using 2D and 3D

782 geodynamic modelling. However, a recent study by Sizova et al. (2015) modelling

783 Eoarchean–Mesoarchean geodynamics (at appropriate mantle temperatures) makes

784 predictions that can explain the variety and complexity of the Archean geological record.

785 These include formation of a pristine granite–greenstone-like crust with dome-and-keel

786 geometry formed over delaminating–upwelling mantle, followed by the development of

787 reworked (accreted) crust that is subjected to both strong horizontal shortening and vertical

788 tectonics processes, which are terminated by short-lived subduction events. These non-

789 uniformitarian models predict the formation of voluminous TTG-like magmas and ultimately

790 produce discrete, shear-zone bounded crustal terranes that resemble the architecture of the

791 Archean rocks within mainland Lewisian Complex.

792

793 *5.3. Future work*

794   Like other areas of Archean crust, unravelling the complexities recorded in the rocks

795 of the Lewisian Complex to reveal their geodynamic evolution is difficult, not least because,

796 despite a large volume of data, the geochemical and geochronological data are ambiguous.

797 Finding some consensus on the absolute timing of 'events' may lie in analysing Sm–Nd and

798 Lu–Hf isotopic composition of garnet and/or U–Pb analysis of zircon/baddeleyite within the

799 mafic rocks. Resolving whether the various crustal blocks are disrupted then reassembled

800 fragments of a single lithosphere unit or are exotic terranes may be resolved using Hf (and

801 other) isotopic measurements of accessory minerals; the acquisition of such data is becoming

802 increasingly faster and cost-effective. In addition, a detailed knowledge of the spatial

803 distribution of Badcallian metamorphic conditions may inform the nature of the proposed

804 terrane boundaries and the potential presence (or otherwise) of belts of rocks recording both

805 higher and lower than average apparent thermal gradients that are a signature of subduction.

806 This requires phase equilibria modelling of tens or hundreds of samples. More detailed

807 mapping of the ultramafic–mafic bodies, brown gneisses and host rocks may provide some

808 information on their early (pre- to syn-Badcallian kinematic history), although subsequent

809 deformation may have destroyed this evidence throughout the Lewisian Complex.

810

811

812 **6. Conclusions**

813

814   The field evidence relating to the large ultramafic–mafic bodies, in particular as it

815 relates to the early structural evolution, has been overprinted by subsequent events and is

816 equivocal. The composition of the rocks is highly variable, probably as a consequence of

817 magmatic differentiation in layered intrusive complexes, subsequent melting during

818 ultrahigh-temperature metamorphism and interaction with neighbouring rocks and partial

819 melts derived therefrom. As a result the geochemical characteristics are not clearly diagnostic

820 of magmatic process or tectonic setting. The 'arc-like' signature exhibited by many Archean

34

821   rocks is not unique to a subduction–accretion environment; there are other mechanisms of

822   enriching mantle source rocks that are perhaps more plausible at the higher temperatures that

823   would have characterised the Archean. Although a subduction origin is possible, we suggest

824   that the layered kilometre- to decametre-scale ultramafic–mafic bodies and associated

825   supracrustal rocks might be the remnants of greenstone belts that sank into partially molten

826   TTG-dominated crust. Whether similar ultramafic–mafic complexes in other high-grade

827   gneiss terrains represent evidence of subduction or were intracratonic should be re-evaluated

828   on a case-by-case basis. However, the possibility that Archean cratonic fragments, which

829   commonly comprise a collage of discrete terranes, could have been produced in a non-plate

830   tectonic scenario is becoming increasingly hard to dismiss (Bédard et al., 2013; Johnson et al,

831   2014; Bédard and Harris, 2014; Sizova et al., 2015; cf. Polat et al., 2015).

832

833

834   **Acknowledgements**

835

836   We thank Jean Bédard, Tim Ivanic, John Percival and anonymous for their reviews

837   and John Wheeler for comments on an earlier version of the manuscript. KG publishes with

838   the permission of the Executive Director of the British Geological Survey.

839

840

841   **References**

842   Anhaeusser, C.R., 1975. Precambrian tectonic environments. Annual Review of Earth and

843   Planetary Sciences, 3, 31–53.

844   Anhaeusser, C.R., 2001. The anatomy of an extrusive-intrusive Archean mafic-ultramafic

845   sequence: the Nelshoogte schist belt and Stolzburg Layered ultramafic complex,

846   Barberton greenstone belt, South Africa. South African Journal of Geology, 104, 167–

847   204.

848   Anhaeusser, C.R., 2014. Archean greenstone belts and associated granitic rocks – A review.

849   Journal of African Earth Sciences, 100, 684–732.

850   Ashwal, L.D., Tucker, R.D., Zinner, E.K., 1999. Slow cooling of deep crustal granulites and

851   Pb-loss in zircon. Geochimica et Cosmochimica Acta, 63, 2839–2851.

852   Barnicoat, A.C., 1983. Metamorphism of the Scourian Complex, NW Scotland, Journal of

853   Metamorphic Geology, 1, 163–182.

854   Beach, A., 1973. The mineralogy of high temperature shear zones at Scourie, NW Scotland.

855   Journal of Petrology, 14, 231–248.

856   Beach, A., 1974. The measurement and significance of displacements on Laxfordian Shear

857   Zones, North-West Scotland. Proceedings of the Geologists' Association, 85, 13–21.

858   Beach, A., 1976. The interrelations of fluid transport, deformation, geochemistry and heat

859   flow in early Proterozoic shear zones in the Lewisian complex. Philosophical

860   Transactions of the Royal Society of London A, 280, 569–604.

861   Beach, A., 1980. Retrogressive metamorphic processes in shear zones with special reference

862   to the Lewisian complex. Journal of Structural Geology, 2, 257–263.

863   Beach, A., Fyfe, W.S., 1972. Fluid transport and shear zones at Scourie, Sutherland –

864   evidence of overthrusting. Contributions to Mineralogy and Petrology, 36, 175–180.

865   Beach, A., Coward, M.P., Graham, R.H., 1974. An interpretation of the structural evolution

866   of the Laxford Front, north west Scotland. Scottish Journal of Geology, 9, 297–308.

867   Bédard, J.H., 2006. A catalytic delamination-driven model for coupled genesis of Archean

868   crust and sub-continental lithospheric mantle. Geochimica et Cosmochimica Acta, 70,

869   1188–1214.

870   Bédard, J. H., Brouillette, P., Madore, L., & Berclaz, A., 2003. Archean cratonization and

871   deformation in the northern Superior Province, Canada: an evaluation of plate tectonic

872   versus vertical tectonic models. Precambrian Research, 127, 61-87.

873   Bédard, J. H., & Harris, L. B., 2014. Neoarchean disaggregation and reassembly of the

874   Superior craton. Geology, 42, 951–954.

875   Bédard, J.H., Harris, L.B., Thurston, P.C., 2013. The hunting of the snArc. Precambrian

876   Research, 229, 20–48.

877   Blewett, R. S., 2002. Archean tectonic processes: a case for horizontal shortening in the

878   North Pilbara Granite-Greenstone Terrane, Western Australia. Precambrian

879   Research, 113, 87–120.

880   Bouhallier, H., Chardon, D., Choukroune, P., 1995. Strain patterns in Archean dome-and-

881   basin structures – the Dharwar craton (Karnataka, south India). Earth and Planetary

882   Science Letters, 135, 57–75.

883   Bowes, D.R., Wright, A.E., Park, R.G., 1964. Layered intrusive rocks in the Lewisian of the

884   North-West Highlands of Scotland. Quarterly Journal of the Geological Society, 120,

885   153–192.

886   Bowes, D.R., Wright, A.E., Park, R.G., 1966. Correspondence. Origin of ultrabasic and basic

887   masses in the Lewisian. Geological Magazine, 103, 280–283.

888   Bremond d'Ars, J.D., Lecuyer, C., Reynard, B., 1999. Hydrothermalism and diapirism in the

889   Archean: gravitational instability constraints. Tectonophysics, 304, 29–39.

890   Brown, M., 2014. The contribution of metamorphic petrology to understanding lithosphere

891   evolution and geodynamics. Geoscience Frontiers, 5, 553-569.

892   Brown, M., 2015. Paleo- to Mesoarchean polymetamorphism in the Barberton Granite-

893   Greenstone Belt, South Africa: Constraints from U-Pb monazite and Lu-Hf garnet

894   geochronology on the tectonic processes that shaped the belt: Discussion. Geological

895   Society of America Bulletin, first published on April 30, 2015, doi:10.1130/B31198.1.

896   Brun, J.P., 1980. The cluster-ridge pattern of mantled gneiss domes in eastern Finland:

897   evidence for large-scale gravitational instability in the Proterozoic crust. Earth and

898   Planetary Science Letters, 44, 441-449.

899   Brun, J.P., Gapais, D., Le Theoff, B., 1981. The mantled gneiss domes of Kuopio (Finland):

900   interfering diapirs. Tectonophysics, 74, 283–304.

901   Burton, K.W., Capmas, F., Birck, J-L, Allègre, C.J., Cohen, A.S., 2000. Resolving

902   crystallisation ages of Archean mafic–ultramafic rocks using the Re–Os isotope system.

903   Earth and Planetary Science Letters, 179, 453–467.

904   Cartwright, I., Barnicoat, A.C., 1986. The generation of quartz-normative melts and

905   corundum-bearing restites by crustal anatexis: petrogenetic modelling based on an

906   example from the Lewisian of North-West Scotland, Journal of Metamorphic Geology,

907   4, 79–99.

908   Cartwright, I., Barnicoat, A.C., 1987. Petrology of Scourian supracrustal rocks and

909   orthogneisses from Stoer, NW Scotland: implications for the geological evolution of

910   the Lewisian complex. In: Park, R. G., Tarney, J. (eds) Evolution of the Lewisian and

911   Comparable Precambrian High Grade Terrains. Geological Society, London, Special

912   Publications, 27, 93–107.

913   Cartwright, I., Fitches, W.R., O'Hara, M.J., Barnicoat, A.C., O'Hara, S., 1985. Archean

914   supracrustal rocks from the Lewisian near Stoer, Sutherland. Scottish Journal of

915   Geology, 21, 187–196.

916   Chardon, D., Choukroune, P., Jayananda, M., 1996. Strain patterns, décollement and

917   incipient sagducted greenstone terrains in the Archean Dharwar craton (south India).

918   Journal of Structural Geology, 18, 991–1004.

919   Chardon, D., Choukroune, P., Jayananda, M., 1998. Sinking of the Dharwar Basin (South

920   India): implications for Archean tectonics. Precambrian Research, 91, 15–39.

921   Cohen, A.S., ONions, R.K., OHara, M.J., 1991. Chronology and mechanism of depletion in

922   Lewisian granulites. Contributions to Mineralogy and Petrology, 106, 142–153.

923   Collins, W.J., Van Kranendonk, M.J., Teyssier, C., 1998. Partial convective overturn of

924   Archean crust in the east Pilbara Craton, Western Australia: driving mechanisms and

925   tectonic implications. Journal of Structural Geology, 20, 1,405–1,424.

926   Condie, K., 2015. Changing tectonic settings through time: Indiscriminate use of

927   geochemical discriminant diagrams. Precambrian Research, 266, 587–591.

928   Corfu, F., Heaman, L.M., Rogers, G., 1994. Polymetamorphic evolution of the Lewisian

929   complex, NW Scotland, as recorded by U-Pb isotopic compositions of zircon, titanite

930   and rutile. Contributions to Mineralogy and Petrology, 117, 215–228.

931   Corfu, F., 2007. Comment to paper: Timing of magmatism and metamorphism in the

932   Gruinard Bay area of the Lewisian gneiss complex: comparison with the Assynt

933   Terrane and implications for terrane accretion by G.J. Love, P.D. Kinny and C.R.L.

934   Friend (Contr Mineral Petrol (2004) 146:620–636). Contributions to Mineralogy and

935   Petrology, 153, 483–488.

936   Coward, M.P., 1984. Major shear zones in the Precambrian crust; examples from NW

937   Scotland and southern Africa and their significance. In: Kröner, A., Greiling, R. (eds)

938   Precambrian Tectonics Illustrated. Stuttgart, Germany, E. Schweizerbart'sche

939   Verlagsbuchhandlung, 207–235.

940   Coward, M.P., 1990. Shear zones at the Laxford Front, NW Scotland and their significance in

941   the interpretation of lower crustal structure. Journal of the Geological Society, London,

942   147, 279–286.

943   Coward, M.P., Park, R.G., 1987. The role of mid-crustal shear zones in the Early Proterozoic

944   evolution of the Lewisian. In: Park, R. G. and Tarney, J. (eds) Evolution of the

945   Lewisian and Comparable Precambrian High Grade Terrains. Geological Society,

946   London, Special Publications, 27, 127–138.

947 Crowley, Q.G., Key, R., Noble, S.R., 2015. High-precision U–Pb dating of complex zircon

948   from the Lewisian Gneiss Complex of Scotland using an incremental CA-ID-TIMS

949   approach. Gondwana Research, 27, 1381–1391.

950 Cutts, K.A., Stevens, G., Kisters, A., 2015. Reply to "Paleo- to Mesoarchean

951   polymetamorphism in the Barberton granite-greenstone belt, South Africa: Constraints

952   from U-Pb monazite and Lu-Hf garnet geochronology on the tectonic processes that

953   shaped the belt: Discussion" by M. Brown. Geological Society of America Bulletin,

954   first published on April 30, 2015, doi:10.1130/B31304.1.

955 Davies, F.B., 1974. A layered basic complex in the Lewisian, south of Loch Laxford,

956   Sutherland. Journal of the Geological Society, London, 130, 279–284.

957 Davies, F.B., 1976. Early Scourian structures in the Scourie-Laxford region and theirbearing

958   on the evolution of the Laxford Front. Journal of the Geological Society, London, 132,

959   543–554.

960 Davies, J.H.F.L., Heaman, L.M., 2014. New U–Pb baddeleyite and zircon ages for the

961   Scourie dyke swarm: A long-lived large igneous province with implications for the

962   Paleoproterozoic evolution of NW Scotland. Precambrian Research, 249, 180–198.

963 De Wit, M.J., Ashwal, L.D., 1997. Greenstone Belts. Oxford, Clarendon Press, ??? pp.

964 Drummond, M. S., & Defant, M. J., 1990. A model for trondhjemite–tonalite–dacite genesis

965   and crustal growth via slab melting: Archean to modern comparisons. Journal of

966   Geophysical Research: Solid Earth, 95(B13), 21503–21521.

967 Evans, C. R., 1965. Geochronology of the Lewisian basement near Lochinver, Sutherland.

968   Nature, 207, 54–55.

969 Evans, C.R., Lambert, R.S.J., 1974. The Lewisian of Lochinver, Sutherland; the type area for

970   the Inverian metamorphism. Journal of the Geological Society, 130, 125–150.

971   Fowler, M.B., 1986. Large-ion lithophile element characteristics of an amphibolite facies to

972   granulite facies transition at Gruinard Bay, North-west Scotland. Journal of

973   Metamorphic Geology, 4. 345–359.

974   François, C., Phillippot, P., Rey, P., Rubatto, D., 2014. Burial and exhumation during

975   Archean sagduction in the East Pilbara Granite-Greenstone Terrane. Earth and

976   Planetary Science Letters, 396, 235–251.

977   Friend, C.R.L., Kinny, P.D., 1995. New evidence for protolith ages of Lewisian granulites,

978   northwest Scotland. Geology, 23, 1027–1030.

979   Friend, C.R.L., Kinny, P.D., 2001. A reappraisal of the Lewisian Gniess Complex:

980   geochronological evidence for its tectonic assembly from disparate terrances in the

981   Proterozoic. Contributions to Mineralogy and Petrology, 142. 198–218.

982   Gale, A., Dalton, C.A., Langmuir, C.H., Su, Y., Schilling, J-G., 2013. The mean composition

983   of ocean ridge basalts. Geochemistry, Geophysics, Geosystems, 14, 489–518.

984   Gapais, D., Jaguin, J., Cagnard, F., Boulvais, P., 2014. Pop-down tectonics, fluid channelling

985   and ore deposits within ancient hot orogens. Tectonophysics, 618, 102–106.

986   Goodenough, K.M., Crowley, Q.G., Krabbendam, M., Parry, S.F., 2013. New U–Pb

987   constraints for the Laxford Shear Zone, NW Scotland: Evidence for tectono-magmatic

988   processes associated with the formation of a Paleoproterozoic supercontinent.

989   Precambrian Research, 233, 1–19.

990   Goodenough, K.M., Park, R.G., Krabbendam, M., Myers, J., Wheeler, J., Loughlin, S.C.,

991   Crowley, Q.G., Friend, C.R.L., Beach, A., Kinny, P.D., Graham, R.H., 2010. The

992   Laxford Shear Zone: an end-Archean terrane boundary? In: Law, R., Butler, R.W.H.,

993   Holdsworth, R.E., Krabbendam, M., Strachan, R. (eds) Continental Tectonics and

994   Mountain Building: The Legacy of Peach and Horne. Geological Society, London,

995   Special Publications, 335, 103–120.

996   Goodwin, A.M., 1991, Precambrian Geology, Academic Press, London, 666 pp.

997   Goodwin, Smith, 1980. Chemical discontinuities in Archean volcanic terrains and the

998   development of Archean crust. Precambrian Research, 10, 301–311.

999   Hamilton, P.J., Evensen, N.M., ONions, R.K., Tarney, J., 1979. Sm-Nd systematics of

1000   Lewisian gneisses: implications for the origin of granulites. Nature, 277, 25–28.

1001   Herzberg, C., Condie, K., Korenaga, J., 2010. Thermal history of the Earth and its

1002   petrological expression. Earth and Planetary Science Letters, 292, 79–88.

1003   Hofmann, A. W., 1988. Chemical differentiation of the Earth: the relationship between

1004   mantle, continental crust, and oceanic crust. Earth and Planetary Science Letters, 90,

1005   297—314.

1006   Horie, K., Nutman, A.P., Friend, C.R.L., Hidaka, H., 2010. The complex age of orthogneiss

1007   protoliths exemplified by the EoArchean Itsaq Gneiss Complex (Greenland): SHRIMP

1008   and old rocks. Precambrian Research, 183, 25–43.

1009   Hughes, H.S.R., McDonald, I, Goodenough, K.M., Ciborowski, T.J.R., Kerr, A.C., Davies,

1010   J.H.F.L., Selby, D., 2014. Enriched lithospheric mantle keel below the Scottish margin

1011   of the North Atlantic Craton: Evidence from the Palaeoproterozoic Scourie Dyke

1012   Swarm and mantle xenoliths. Precambrian Research, 250, 97–126.

1013   Irvine, A.J., Baragar, W.R.A., 1971. A guide to the chemical classification of the common

1014   volcanic rocks. Canadian Journal of Earth Sciences, 8, 523–548.

1015   Jenner, F. E., Bennett, V. C., Nutman, A. P., Friend, C. R., Norman, M. D., Yaxley, G., 2009.

1016   Evidence for subduction at 3.8 Ga: geochemistry of arc-like metabasalts from the

1017   southern edge of the Isua Supracrustal Belt. *Chemical Geology*, *261*, 83–98.

1018   Johnson, T.E., Brown, M., Kaus, B., VanTongeren, J.A., 2014. Delamination and recycling

1019   of Archean crust caused by gravitational instabilities. Nature Geoscience, 7, 47–52.

1020   Johnson, T.E., Fischer, S., White, R.W., 2013. Field and petrographic evidence for partial

1021   melting of TTG gneiss within the central region of the mainland Lewisian complex,

1022   NW Scotland. Journal of the Geological Society, London, 170, 319–326.

1023   Johnson, T.E., Fischer, S., White, R.W., Brown, M., Rollinson, H.R., 2012. Archean

1024   intracrustal differentiation from partial melting of metagabbro – field and geochemical

1025   evidence from the central region of the Lewisian complex, NW Scotland. Journal of

1026   Petrology, 53, 2115–2138.

1027   Johnson, T.E., White, R.W., 2011. Phase equilibrium constraints on conditions of granulite-

1028   facies metamorphism at Scourie, NW Scotland. Journal of the Geological Society,

1029   London, 168, 147–158.

1030   Kerrich, R., Polat, A., Wyman, D., Hollings, P., 1999. Trace element systematics of Mg-, to

1031   Fe-tholeiitic basalt suites of the Superior Province: implications for Archean mantle

1032   reservoirs and greenstone belt genesis. Lithos, 46, 163-187.

1033   Kinny, P.D., Friend, C.R.L., 1997. U–Pb isotopic evidence for the accretion of different

1034   crustal blocks to form the Lewisian complex of northwest Scotland. Contributions to

1035   Mineralogy and Petrology, 129, 326–340.

1036   Kinny, P.D., Friend, C.R.L., Love, G.J., 2005. Proposal for a terrane-based nomenclature for

1037   the Lewisian Gneiss Complex of NW Scotland. Journal of the Geological Society,

1038   London, 162. 175–186.

1039   Kisters, A. F., & Anhaeusser, C. R., 1995. Emplacement features of Archean TTG plutons

1040   along the southern margin of the Barberton greenstone belt, South Africa. Precambrian

1041   Research, 75, 1–15.

1042   Kisters, A.F.M., Stevens, G., Dziggel, A., Armstrong, R.A., 2003. Extensional detachment

1043   faulting and core-complex formation in the southern Barberton granite–greenstone

1044   terrain, South Africa: Evidence for a 3.2 Ga orogenic collapse: Precambrian Research,

1045   127, 355–378.

1046   Kisters, A.F.M., Belcher, R.W., Poujol, M., Dziggel, A., 2010. Continental growth and

1047   convergence-related arc plutonism in the MesoArchean: Evidence from the Barberton

1048   granitoid–greenstone terrain, South Africa: Precambrian Research, 178, 15–26.

1049   Kuno, H., 1968. Differentiation of basalt magma. In: Hess, H.H., Poldervaart, A. (eds),

1050   Basalts: The Poldervaart treatise on rocks of basaltic composition, Vol. 2. Interscience,

1051   New York, pp. 623–688.

1052   Le Maitre, R.W., Streckeisen, A., Zanettin, B., Le Bas, M.J., et al., 2002. Igneous Rocks: A

1053   Classification and Glossary of Terms, Recommendations of the International Union of

1054   Geological Sciences. Cambridge University Press, Cambridge, UK.

1055   Li, C., Arndt, N.T., Tang, Q., Ripley, E.M., 2015. Trace element indiscrimination diagrams.

1056   Lithos, 232, 76–83.

1057   Lin, S., Beakhouse, G.P., 2013. Synchronous vertical and horizontal tectonism at late stages

1058   of Archean cratonization and genesis of Hemlo gold deposit, Superior craton, Ontario,

1059   Canada. Geology, 41, 359–362.

1060   Liou, J.G., Tsujimori, T., Yang, J., Zhang, R.Y., Ernst, W.G., 2014. Recycling of crustal

1061   materials through study of ultrahigh-pressure minerals in collisional orogens,

1062   ophiolites, and mantle xenoliths: A review. Journal of Asian Earth Sciences, 96, 386–

1063   420.

1064   Love, G., Kinny, P., Friend, C., 2004. Timing of magmatism and metamorphism in the

1065   Gruinard Bay area of the Lewisian Gneiss Complex: comparisons with the Assynt

1066   Terrane and implications for terrane accretion. Contributions to Mineralogy and

1067   Petrology, 146, 620–636.

1068   MacDonald, J.M., Wheeler, J., Harley, S.L., Mariani, E., Goodenough, K.M., Crowley, Q.,

1069   Tatham, D., 2013. Lattice distortion in a zircon population and its effects on trace

1070   element mobility and U–Th–Pb isotope systematics: examples from the Lewisian

1071   Gneiss Complex, northwest Scotland. Contributions to Mineralogy and Petrology, 166,

1072   21–41.

1073 Marshak, S., 1999. Deformation style way back when: thoughts on the contrasts between

1074   Archean/Paleoproterozoic and contemporary orogens. Journal of Structural Geology,

1075   21, 1175–1182.

1076 Martin, H., Moyen, J.-F, Guitreau, M., Blichert-Toft, J., Le Pennec, J.-L., 2014. Why

1077   Archean TTG cannot be generated by MORB melting in subduction zones. Lithos,

1078   198–199, 1–13.

1079 Mason, A. J., 2015. The Palaeoproterozoic anatomy of the Lewisian Complex, NW Scotland:

1080   evidence for two 'Laxfordian' tectonothermal cycles. Journal of the Geological Society,

1081   xx, xxx–xxx.

1082 McDonough, W.F., Sun, S.-s., 1995. The composition of the Earth. Chemical Geology, 120,

1083   223–253.

1084 McGregor, A.M., 1951. Some milestones in the Precambrian of Southern Rhodesia.

1085   Geological Society of South Africa Transactions and Proceedings, 54, 27–71.

1086 Moorbath, S., Welke, H., Gale, N., 1969. The significance of lead isotope studies in ancient,

1087   high-grade metamorphic basement complexes, as exemplified by the Lewisian rocks of

1088   Northwest Scotland. Earth and Planetary Science Letters, 6, 245–256.

1089 Moyen, J.-F., 2011. The composite Archean grey gneisses: Petrological significance, and

1090   evidence for a non-unique tectonic setting for Archean crustal growth. Lithos, 123, 21–

1091   36.

1092 Moyen, J.-F., Martin, H., 2012. Forty years of TTG research. Lithos, 148, 312-336.

1093 Myers, J. S., Watkins, K. P., 1985. Origin of granite–greenstone patterns, Yilgarn Block,

1094   Western Australia. Geology, 13, 778–780.

1095 Nutman, A.P., Bennett, V.C., Friend, C.R.L., Hidaka, H., Yi, K., Lee, S.R., Kamiichi, T.,

1096   2013. The Itsaq gneiss complex of Greenland: episodic 3900 to 3660 Ma juvenile crust

1097   formation and recycling in the 3660 to 3600 Ma Isukasian orogeny. American Journal

1098   of Science, 313, 877–911.

1099   Nutman, A.P., Bennett, V.C., Friend, C.R.L., 2015. The emergence of the Eoarchaean proto-

1100   arc: evolution of a c. 3700 Ma convergent plate boundary at Isua, southern West

1101   Greenland. Geological Society Special Publication, 389, 113–133.

1102   O'Hara, M.J., 1961. Zoned Ultrabasic and Basic Gneiss Masses in the Early Lewisian

1103   Metamorphic Complex at Scourie, Sutherland. Journal of Petrology, 2, 248–276.

1104   O'Hara, M.J., 1965. Origin of ultrabasic and basic masses in the Lewisian. Geological

1105   Magazine, 102, 296–314.

1106   O'Hara, M.J., 1966. Correspondence. Origin of ultrabasic and basic masses in the Lewisian.

1107   Geological Magazine, 103, 284.

1108   O'Hara, M.J., Yarwood, G., 1978. High pressure–temperature point on an Archean geotherm,

1109   implied magma genesis by crustal anatexis, and consequences for garnet-pyroxene

1110   thermometry and barometry. Philosophical Transactions of the Royal Society of

1111   London. Series A, Mathematical and Physical Sciences, 288, 441–456.

1112   O'Nions, R. K., Hamilton, P. J., & Hooker, P. J., 1983. A Nd isotope investigation of

1113   sediments related to crustal development in the British Isles. Earth and Planetary

1114   Science Letters, 63, 229–240.

1115   Ordóñez-Calderón, J.C., Polat, A., Fryer, B.J., Gagnon, J.E., 2011. Field and geochemical

1116   characteristics of Mesoarchean to Neoarchean volcanic rocks in the Storø greenstone

1117   belt, SW Greenland: Evidence for accretion of intra-oceanic volcanic arcs. Precambrian

1118   Research, 184, 24-42.

1119   Qian, Q., Hermann, J., 2013. Partial melting of lower crust at 10–15 kbar: constraints on

1120   adakite and TTG formation. Contributions to Mineralogy and Petrology, 165, 1195–

1121   1224.

1122   Park, R.G., 2005. The Lewisian terrane model: a review. Scottish Journal of Geology, 41,

1123   105–118.

1124   Park, R.G., 1970. Observations on Lewisian Chronology. Scottish Journal of Geology, 6,

1125   379–399.

1126   Park, R.G., Tarney, J., 1987. The Lewisian complex: a typical Precambrian high-grade

1127   terrain? In: Park, R. G., Tarney, J. (eds) Evolution of the Lewisian and Comparable

1128   Precambrian High Grade Terrains. Geological Society, London, Special Publications,

1129   27, 13–25.

1130   Park, R.G., Tarney, J., Connelly, J. N., 2001. The Loch Maree Group: Palaeoproterozoic

1131   subduction-accretion complex in the Lewisian of NW Scotland. Precambrian Research,

1132   105, 205–226.

1133   Parmenter, A.C., Lin, S.F., Corkery, M.T., 2006. Structural evolution of the Cross Lake

1134   greenstone belt in the northwestern Superior Province, Manitoba: implications for

1135   relationship between vertical and horizontal tectonism. Canadian Journal of Earth

1136   Sciences, 43, 767–787.

1137   Peach, B. N., Horne, J., Gunn, W., Clough, C. T., Hinxman, L. W., Teall, J. J. H., 1907. The

1138   Geological Structure of the North West Highlands of Scotland, Memoirs of the

1139   Geological Survey of Great Britain.

1140   Pearce, J.A., 2008. Geochemical fingerprinting of oceanic basalts with applications to

1141   ophiolite classification and the search for Archean oceanic crust. Lithos, 100, 14–48.

1142   Pearce, J.A., 2014a. Geochemical Fingerprinting of the Earth's Oldest Rocks. Geology, 42,

1143   175–176.

1144   Pearce, J.A., 2014b. Immobile element fingerprinting of ophiolites. Elements, 10, 101–108.

1145   Pearce, J.A., Cann, J.R., 1973. Tectonic setting of basic volcanic rocks determined using

1146   trace element analyses. Earth and Planetary Science Letters, 19, 290–300.

1147 Pearce, J.A., Peate, D.W., 1995. Tectonic implications of the composition of volcanic arc

1148   magmas. Annual Review of Earth and Planetary Sciences, 23, 251–285.

1149 Polat, A., 2009. The geochemistry of Neoarchean (ca. 2700 Ma) tholeiitic basalts, transitional

1150   to alkaline basalts, and gabbros, Wawa Subprovince, Canada: Implications for

1151   petrogenetic and geodynamic processes. Precambrian Research, 168, 83-105.

1152 Polat, A., Wang, L., Appel, P. W., 2015. A review of structural patterns and melting

1153   processes in the Archean craton of West Greenland: Evidence for crustal growth at

1154   convergent plate margins as opposed to non-uniformitarian models. Tectonophysics,

1155   xx, xxx–xxx.

1156 Pride, C., Muecke, G.K., 1982. Geochemistry and origin of granitic rocks, Scourian

1157   Complex, NW Scotland. Contributions to Mineralogy and Petrology, 80. 379–385.

1158 Pride, C., Muecke, G.K., 1980. Rare earth element geochemistry of the Scourian complex

1159   N.W. Scotland – Evidence for the granite-granulite link. Contributions to Mineralogy

1160   and Petrology, 73, 403–412.

1161 Ramsay, J.G., 1989. Emplacement kinematics of a granite diapir: the Chindamora batholith,

1162   Zimbabwe. Journal of Structural Geology, 11, 191–209.

1163 Rapp, R. P., Shimizu, N., & Norman, M. D., 2003. Growth of early continental crust by

1164   partial melting of eclogite. Nature, 425, 605–609.

1165 Robin, C.M.I., Bailey, R.C., 2009. Simultaneous generation of Archean crust and subcratonic

1166   roots by vertical tectonics. Geology, 37, 523–526.

1167 Rollinson, H.R., 1996. Tonalite-trondhjemite-granodiorite magmatism and the genesis of

1168   Lewisian crust during the Archean. In: Brewer, T.S. (ed). Precambrian Crustal

1169   Evolution in the North Atlantic Region. Geological Society, London, Special

1170   Publications, 112, 25–42.

1171 Rollinson, H., 2012. Geochemical constraints on the composition of Archean lower

1172   continental crust: Partial melting in the Lewisian granulites. Earth and Planetary

1173   Science Letters, 351–352, 1–12.

1174 Rollinson, H.R., Fowler, M.B., 1987. The magmatic evolution of the Scourian complex at

1175   Gruinard Bay. In: Park, R. G. and Tarney, J. (eds) Evolution of the Lewisian and

1176   Comparable Precambrian High Grade Terrains. Geological Society, London, Special

1177   Publications, 27, 57–71.

1178 Rollinson, H.R., Gravestock, P., 2012. The trace element geochemistry of clinopyroxenes

1179   from pyroxenites in the Lewisian of NW Scotland: insights into light rare earth element

1180   mobility during granulite facies metamorphism. Contributions to Mineralogy and

1181   Petrology, 163, 319–335.

1182 Rollinson, H.R., Tarney, J., 2005. Adakites – the key to understanding LILE depletion in

1183   granulites. Lithos, 79, 61–81.

1184 Rollinson, H.R., Windley, B.F., 1980. An Archean granulite-grade tonalite–trondhjemite–

1185   granite suite from Scourie, NW Scotland: Geochemistry and origin. Contributions to

1186   Mineralogy and Petrology, 72, 265–281.

1187 Sandiford, M., Kranendonk, M.V., Bodorkos, S., 2004. Conductive incubation and the origin

1188   of Granite-Greenstone dome-and-keel structure: the eastern Pilbara Craton. Tectonics,

1189   23, TC1009, doi:10.1029/2002TC001452.

1190 Sajeev, K., Windley, B.F., Hegner, E., Komiya, T., 2013. High-temperature, high-pressure

1191   granulites (retrogressed eclogites) in the central region of the Lewisian, NW Scotland:

1192   Crustal-scale subduction in the NeoArchean. Gondwana Research, 23, 526–538.

1193 Sheraton, J.W., Tarney, J., Wheatley, T.J., Wright, A.E., 1973. The Structural History of the

1194   Assynt district. In: Park, R.G and Tarney, J. (eds) The Early Precambrian of Scotland

1195   and Related Rocks of Greenland. University of Keele, pp. 31–43.

1196   Sills, J.D., 1983. Mineralogical changes occurring during the retrogression of Archean

1197   gneisses from the Lewisian complex of NW Scotland. Lithos, 16, 113–124.

1198   Sills, J.D., Rollinson, H.R., 1987. Metamorphic evolution of the mainland Lewisian complex.

1199   In: Park, R. G. and Tarney, J. (eds) Evolution of the Lewisian and Comparable

1200   Precambrian High Grade Terrains. Geological Society, London, Special Publications,

1201   27, 81–92.

1202   Sills, J.D., Savage, D., Watson, J.V., Windley, B.F., 1982. Layered ultramafic-gabbro bodies

1203   in the Lewisian of northwest Scotland: geochemistry and petrogenesis, Earth and

1204   Planetary Science Letters, 58, 345–360.

1205   Snow, C., 2006. A reevaluation of tectonic discrimination diagrams and a new probabilistic

1206   approach using large geochemical databases: moving beyond binary and ternary plots.

1207   Journal of Geophysical Research, 111, http://dx.doi.org/10.1029/2005JB003799

1208   (B06206).

1209   Sizova, E., Gerya, T., Stüwe, K., Brown, M., 2015. Generation of felsic crust in the Archean:

1210   a geodynamic modeling perspective. Precambrian Research, revised awaiting

1211   acceptance.

1212   Sun, S.s., McDonough, W.F., 1989. Chemical and isotopic systematics of oceanic basalts:

1213   implications for mantle composition and processes. In: Saunders, A.D., Norry, M.J.

1214   (eds) Magmatism in the Ocean Basins. Geological Society, London, Special

1215   Publications, 42, 313–345.

1216   Sutton, J., Watson, J., 1951. The pre-Torridonian metamorphic history of the Loch Torridon

1217   and Scourie areas in the North-West Highlands, and its bearing on the chronological

1218   classification of the Lewisian. Quarterly Journal of the Geological Society, 106, 241–

1219   307.

1220   Tatsumi, Y. (2005). The subduction factory: how it operates in the evolving Earth. *GSA*

1221   *today*, *15*, 4.

1222   Thebaud, N., Rey, P.F., 2013. Archean gravity-driven tectonics on hot and flooded

1223   continents: Controls on long-lived mineralised hydrothermal systems away from

1224   continental margins. Precambrian Research, 229, 93–104.

1225   Van Kranendonk, M.J., Collins, W.J., Hickman, A., Pawley, M.J., 2004. Critical tests of

1226   vertical vs. horizontal tectonic models for the Archean East Pilbara Granite-Greenstone

1227   Terrane, Pilbara Craton, Western Australia. Precambrian Research, 131, 173–211.

1228   Van Kranendonk, M.J., Kröner, A., Hoffman, E.J., Nagel, T., Anhaeusser, C.R., 2014. Just

1229   another drip: re-analysis of a proposed Mesoarchean suture from the Barberton

1230   Mountain Land, South Africa. Precambrian Research, 254, 19–35.

1231   Walter, M.J., 1998. Melting of Garnet Peridotite and the Origin of Komatiite and Depleted

1232   Lithosphere. Journal of Petrology, 39, 29–60.

1233   Weaver, B.L., Tarney, J., 1980. Rare earth geochemistry of Lewisian granulite-facies

1234   gneisses, northwest Scotland: Implications for the petrogenesis of the Archean lower

1235   continental crust. Earth and Planetary Science Letters, 51, 279–296.

1236   Wellman, P., 2000. Upper crust of the Pilbara Craton, Australia; 3D geometry of a

1237   granite/greenstone terrain. Precambrian Research, 104, 175–186.

1238   Wheeler, J., 2007. A major high strain zone in the Lewisian Complex in the Loch Torridon

1239   area, NW Scotland: insights into deep crustal deformation. In: Ries, A.C., Butler,

1240   R.W.H., Graham, R.H. (eds) Deformation of the Continental Crust: The Legacy of

1241   Mike Coward. Geological Society, London, Special Publications, 272, 27–45.

1242   Wheeler, J., Park, R.G., Rollinson, H.R., Beach, A., 2010. The Lewisian Complex: insights

1243   into deep crustal evolution. In: Law, R., Butler, R.W.H., Holdsworth, R.E.,

1244   Krabbendam, M., Strachan, R. (eds) Continental Tectonics and Mountain Building: The

1245   Legacy of Peach and Horne. Geological Society, London, Special Publications, 335,

1246   51–79.

1247   Whitehouse, M.J., 1989. Sm–Nd evidence for diachronous crustal accretion in the Lewisian

1248   complex of northwest Scotland. Tectonophysics, 161, 245–256.

1249   Whitehouse, M.J., Claesson, S., Sunde, T., Vestin, J., 1997. Ion microprobe U-Pb zircon

1250   geochronology and correlation of Archean gneisses from the Lewisian Complex of

1251   Gruinard Bay, northwestern Scotland. Geochimica et Cosmochimica Acta, 61, 4429–

1252   4438.

1253   Whitehouse, M.J., Fowler, M.B., Friend, C.R.L., 1996. Conflicting mineral and whole-rock

1254   isochron ages from the Late-Archean Lewisian complex of northwestern Scotland:

1255   Implications for geochronology in polymetamorphic high-grade terrains. Geochimica et

1256   Cosmochimica Acta, 60, 3085–3102.

1257   Whitehouse, M.J., Kemp, A.I.S., 2010. On the difficulty of assigning crustal residence,

1258   magmatic protolith and metamorphic ages to Lewisian granulites: constraints from

1259   combined in situ U-Pb and Lu-Hf isotopes. In: Law, R., Butler, R.W.H., Holdsworth,

1260   R.E., Krabbendam, M., Strachan, R. (eds) Continental Tectonics and Mountain

1261   Building: The Legacy of Peach and Horne. Geological Society, London, Special

1262   Publications, 335, 81–101.

1263   Windley, B. F., Bridgwater, D., 1971. The evolution of Archean low- and high-grade terrains.

1264   Geological Society of Australia, Special Publication, 3, 33–46.

1265   Windley, B. F., Smith, J.V., 1971. Archean high-grade complexes and modern continental

1266   margins. Nature, 260, 671–675.

1267   Zhang, C., Holtz, F., Koepke, J., Wolff, P.E., Ma, C., Bédard, J.H., 2013. Constraints from

1268   experimental melting of amphibolite on the depth of formation of garnet-rich restites,

1269   and implications for models of Early Archean crustal growth. Precambrian Research,

1270   231, 206–217.

1271   Zhu, Z.K., O'Nions, R.K., Belshaw, N.S., Gibb, A.J., 1997. Lewisian crustal history from in

1272   situ SIMS mineral chronometry and related metamorphic textures. Chemical Geology,

1273   136, 205–218.

1274   Zirkler, A., Johnson, T.E., White, R.W., Zack, T., 2012. Polymetamorphism in the mainland

1275   Lewisian complex, NW Scotland – phase equilibria and geochronological constraints

1276   from the Cnoc an t'Sidhean suite. Journal of Metamorphic Geology, 30, 865.

1277 **Figure captions**

1278

1279 **Fig. 1.** A simplified geological map of the mainland Lewisian Complex of northwest

1280 Scotland. The complex is traditionally subdivided into a granulite facies central region

1281 bounded by the mainly amphibolite facies northern and southern regions. The more recent

1282 terrane-based nomenclature is also shown (the Gruinard and Assynt terranes in the center,

1283 with the Rhiconich terrane to the north and the Gairloch, Ialltaig and Rona terranes to the

1284 south; Kinny et al., 2005). The position of key localities discussed in the text is indicated.

1285

1286 **Fig. 2.** (a) Geological map, reproduced with permission of the BGS (Innovation agreement

1287 IPR/156–04CL), showing the distribution of the main rocks types in the northwestern part of

1288 the central region (Assynt block), across the Laxford Shear Zone (LSZ) and into the

1289 southwesternmost part of the northern region (Rhiconich block). The map is based on recent

1290 BGS mapping with the location of additional ultramafic–mafic bodies from fig. 1 of Davies

1291 (1976) superimposed (dashed boundaries). The boundaries of the LSZ (approximate positions

1292 shown by the two thick dotted grey lines) trend WNW–ESE and pass through the middle of

1293 Loch Laxford in the north and 2–3 km northeast of Scourie in the south, where the strain

1294 gradient declines and the strain becomes localized in discrete shear zones. The precise

1295 junction between the central and northern regions is unclear. West and south of the Laxford

1296 granites, a prominent belt of large layered ultramafic–mafic bodies is spatially associated

1297 with brown gneisses that occur in synformal cores. By contrast, many of the more isolated

1298 layered bodies, for instance around Scourie, have no clear association with brown gneiss. The

1299 schematic cross-section (b), redrafted from Davies (1976), was drawn along the line A–B

1300 indicated on the map.

1301

1302   **Fig. 3.** Timeline based on data cited in the main text summarising the age constraints on

1303   Archean to Paleoproterozoic 'events' within the central region of the mainland Lewisian

1304   Complex.

1305

1306   **Fig. 4.** (a) Generalized stratigraphy of the layered ultramafic–mafic bodies and associated

1307   supracrustal rocks; (b) Field photographs of typical occurrences of the various units shown in

1308   (a); (c) Chondrite-normalised REE patterns of the various units shown in (a) and (b). In (c),

1309   the grey background field for the brown gneisses shows the range of compositions of

1310   petrographically similar garnet–biotite gneisses from the Storø greenstone belt, SW

1311   Greenland (Ordóñez-Calderón et al., 2011). The grey background field for the ultramafic

1312   rocks shows the range of REE compositions for ~200 komatiites from greenstone belts in the

1313   Superior Province taken from the GEOROC database (http://georoc.mpch-mainz.gwdg.de/).

1314

1315   **Fig. 5.** Variation diagrams showing major oxide compositions of the main lithologies plotted

1316   against MgO (as wt%). The compositions of Archean non-arc basalts, Archean basalts from

1317   the Superior and North Atlantic cratons (SNAC basalts), N-MORB and fertile mantle

1318   composition KR–4003 are shown for reference, along with the average composition of

1319   olivine (ol) and clinopyroxene (cu) from a metamorphosed ultramafic rock and of

1320   clinopyroxene (cm) from a metabasic rock – see main text for further details.

1321

1322   **Fig. 6.** (a) AFM diagram showing the boundaries between the tholeiitic and calc-alkaline

1323   fields proposed by Kuno (1968) and Irvine and Baragar (1971). The ultramafic and metabasic

1324   rocks define a low-alkali trend with strong enrichment in Fe that is characteristic of tholeiitic

1325   magmas. (b) TAS diagram showing the compositions of the metabasic rocks and brown

1326   gneisses.

1327

1328   **Fig. 7.** Representative trace element compositions of the main lithologies normalised to

1329   primitive mantle values of McDonough & Sun (1995). The grey areas show the fields for

1330   particular reference compositions described in the text.

1331

1332   **Fig. 8.** Change in the major (Si to K as oxides) and trace element composition of the average

1333   metabasic rock relative to the average SNAC basalt. Many of these features (e.g. a depletion

1334   in K, Na and most trace elements) are consistent with partial melting and melt loss. Others

1335   (e.g. the pronounced depletion in Ti, Nb and Ta) probably reflect source characteristics (e.g.

1336   Rollinson, 2012).

1337

1338   **Fig. 9.** Trace element discrimination diagrams: (a) Nb/Y vs Ti/Y; (b) Nb/Yb vs Th/Yb; (c)

1339   Nb/Yb vs TiO_2/Yb.

1340

1341

1342

1343

1344

1345   Highlights
1346
1347

1348   • The Lewisian Complex contains large layered ultramafic–mafic bodies and

1349   structurally overlying garnet-biotite gneiss whose origin is unclear

1350   • The rocks have 'arc-like' geochemical signatures that may not be unique to a

1351   subduction environment

1352   • The ultramafic–mafic rocks and brown gneisses may represent the remnants of

1353   intracratonic greenstone belts that sank into the deep crust due to their density contrast

1354   with the underlying partially molten low viscosity TTG orthogneisses

1355

1356
1357

Figure 1

a.

Handa
Island
(Torridonian
sandstone)

Tarbet

Scourie Bay

Scourie

38

Badcall Bay

Loch Laxford

Gorm
Chnoc

LAXFORD SHEAR ZONE

Laxfordian granite
Scourie dyke
Brown schist
Ultramafic–mafic body
TTG orthogneiss
1 km

b.

A   B

from Davies (1976)
no vertical exaggeration
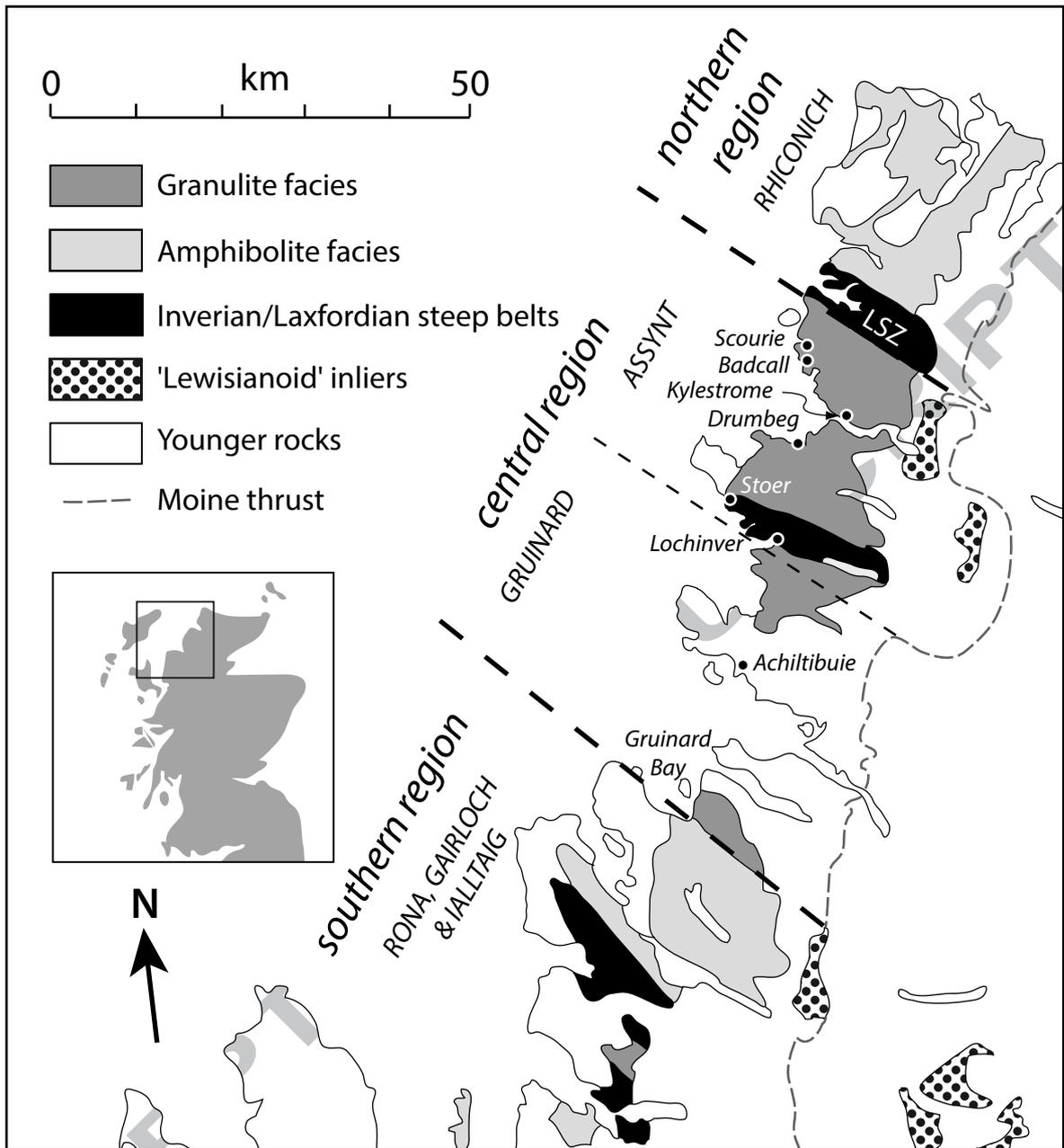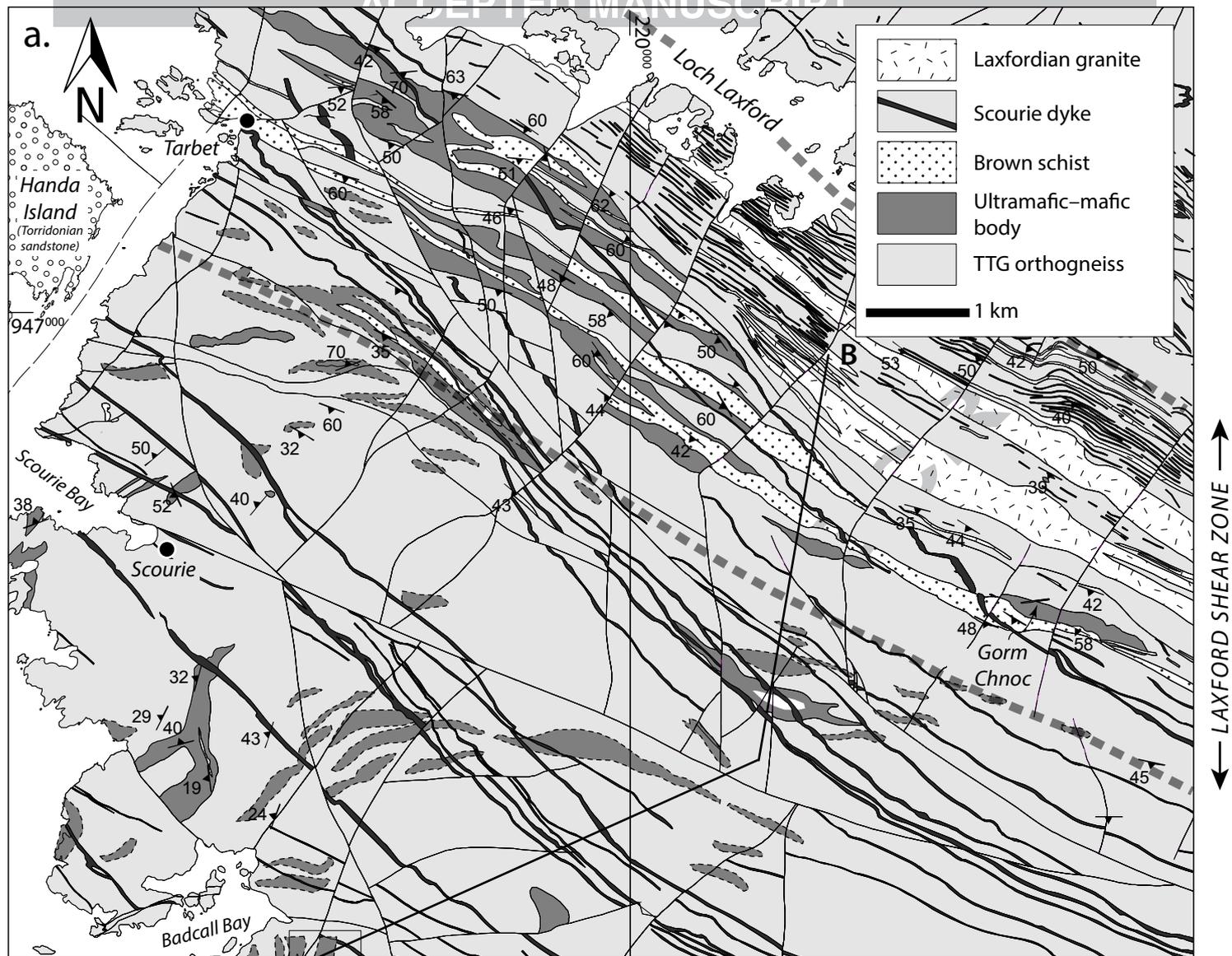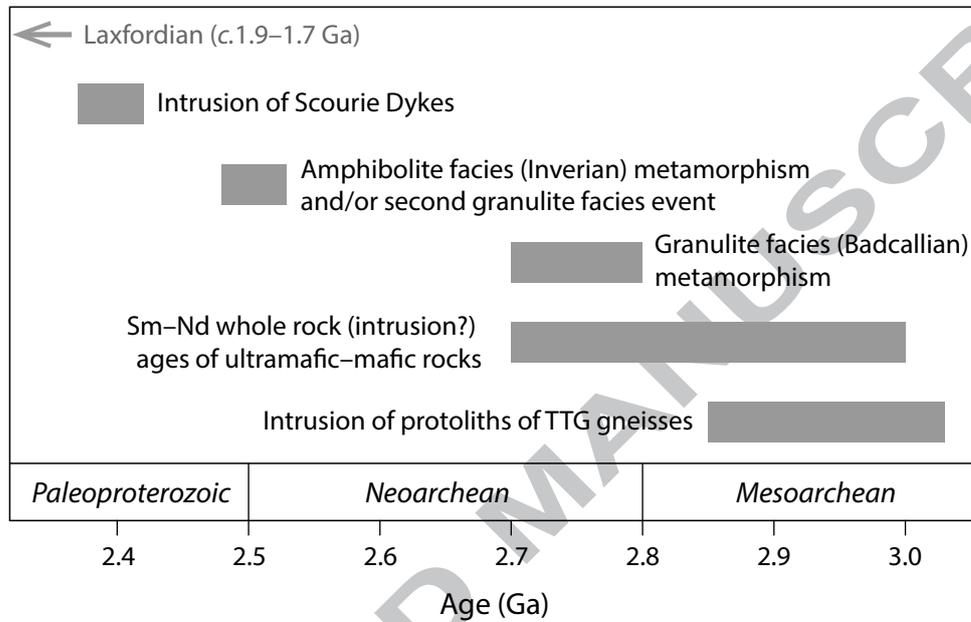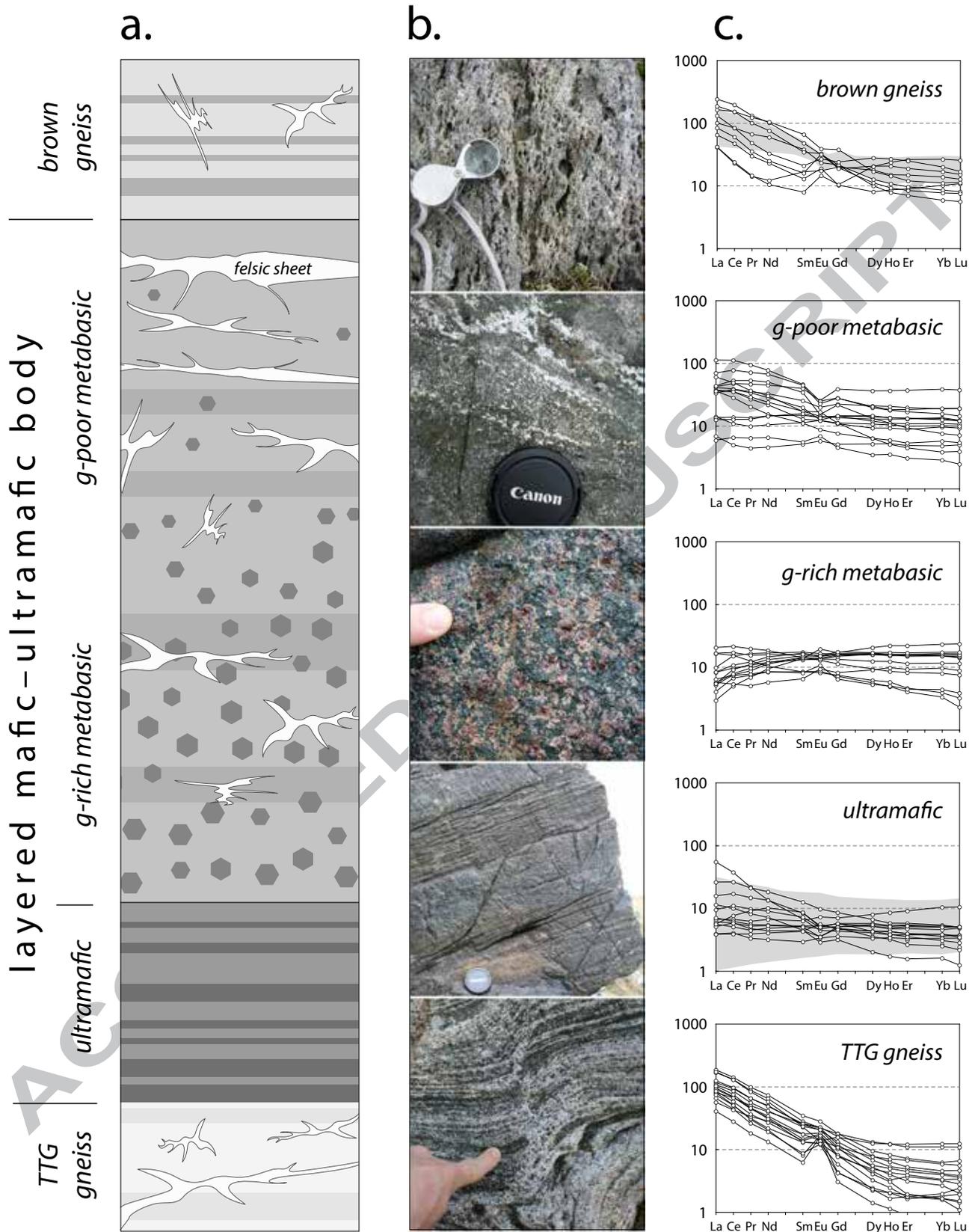
Figure 2

Figure 3

Figure 4
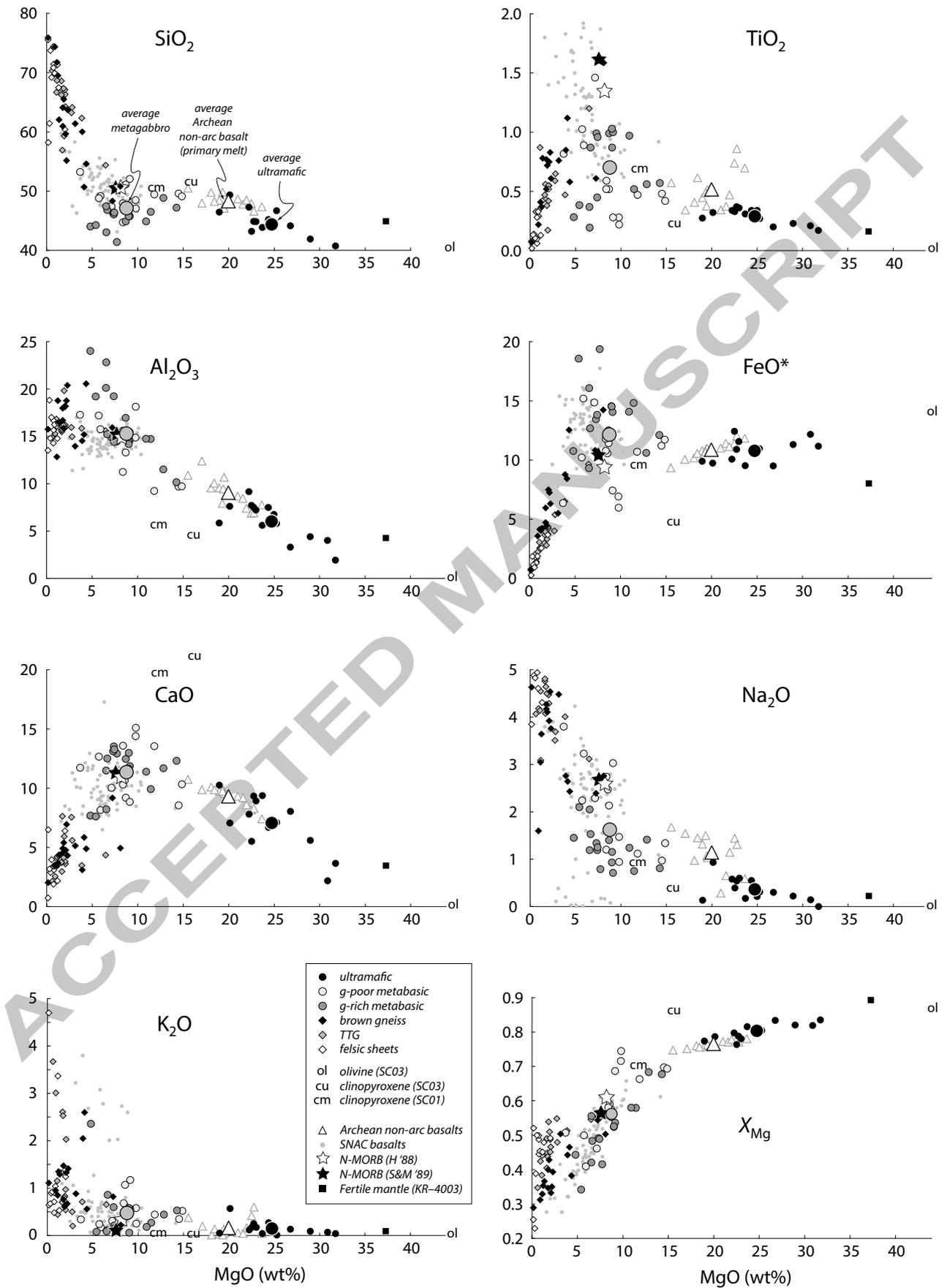
Figure 5
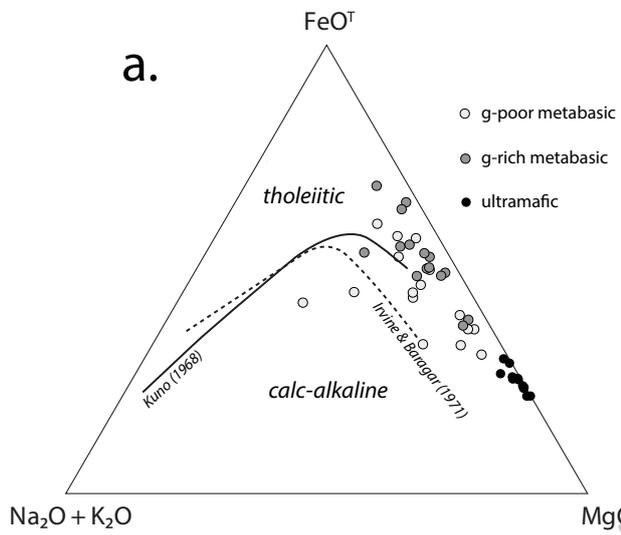
Figure 5
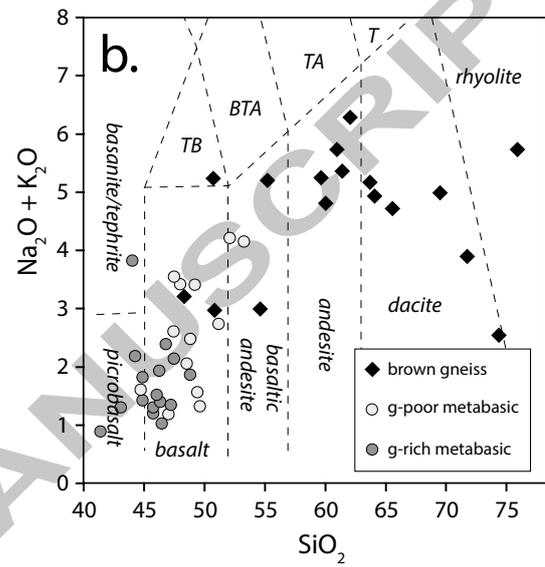
Figure 6
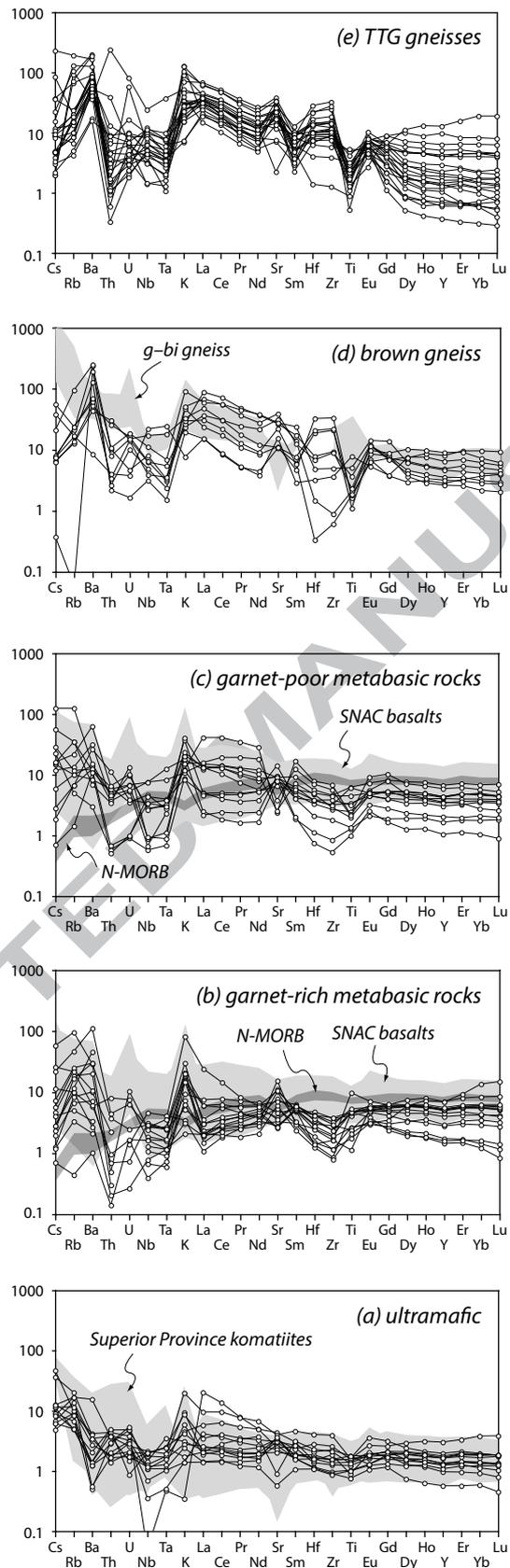
Figure 7

Figure 8

Figure 9